$^{40}Ar/^{39}Ar$ geochronology, isotope geochemistry (Sr, Nd, Pb), and petrology of alkaline lavas near Yampa, Colorado: Migration of alkaline volcanism and evolution of the northern Rio Grande rift

M.A. Cosca, R.A. Thompson, J.P. Lee, K.J. Turner, L.A. Neymark, and W.R. Premo
U.S. Geological Survey, Box 25046, Denver Federal Center, Denver, Colorado 80225, USA

ABSTRACT

Volcanic rocks near Yampa, Colorado (USA), represent one of several small late Miocene to Quaternary alkaline volcanic fields along the northeast margin of the Colorado Plateau. Basanite, trachybasalt, and basalt collected from six sites within the Yampa volcanic field were investigated to assess correlations with late Cenozoic extension and Rio Grande rifting. In this paper we report major and trace element rock and mineral compositions and Ar, Sr, Nd, and Pb isotope data for these volcanic rocks. High-precision $^{40}Ar/^{39}Ar$ geochronology indicates westward migration of volcanism within the Yampa volcanic field between 6 and 4.5 Ma, and the Sr, Nd, and Pb isotope values are consistent with a primary source in the Proterozoic subcontinental lithospheric mantle. Relict olivine phenocrysts have Mg- and Ni-rich cores, whereas unmelted clinopyroxene cores are Na and Si enriched with finely banded Ca-, Mg-, Al-, and Ti-enriched rims, thus tracing their crystallization history from a lithospheric mantle source region to one in contact with melt prior to eruption. A regional synthesis of Neogene and younger volcanism within the Rio Grande rift corridor, from northern New Mexico to southern Wyoming, supports a systematic overall southwest migration of alkaline volcanism. We interpret this Neogene to Quaternary migration of volcanism toward the northeast margin of the Colorado Plateau to record passage of melt through subvertical zones within the lithosphere weakened by late Cenozoic extension. If the locus of Quaternary alkaline magmatism defines the current location of the Rio Grande rift, it includes the Leucite Hills, Wyoming. We suggest that alkaline volcanism in the incipient northern Rio Grande rift, north of Leadville, Colorado, represents melting of the subcontinental lithospheric mantle in response to transient infiltration of asthenospheric mantle into deep, subvertical zones of dilational crustal weakness developed during late Cenozoic extension that have been migrating toward, and subparallel to, the northeast margin of the Colorado Plateau since the middle Miocene. Quaternary volcanism within this northern Rio Grande rift corridor is evidence that the rift is continuing to evolve.

INTRODUCTION

Latest middle Miocene and younger syntransform extension within the southern Basin and Range province (western USA, northwestern Mexico) is related to rapid migration of the Rivera triple junction past Baja Mexico to its current location between the tip of the Baja peninsula and mainland Mexico (Fig. 1; Dickinson, 2004). Evidence of this triple junction migration can be traced to late Cenozoic extension along the eastern margin of the Colorado Plateau, where the Neogene Rio Grande rift forms a prong of the Basin and Range (e.g., Prodehl and Lipman, 1989). Although the physiographic rift graben ends near Leadville, Colorado (Fig. 2), extensional deformation structures including high-angle block faulting and small, low-relief grabens filled with Miocene sedimentary rock of the Browns Park Formation continue west of the Gore and Park Ranges into Wyoming (Izett, 1975; Larson et al., 1975; Tweto, 1979). Locally, these extended areas are associated with late Cenozoic volcanic eruptions and volcanic fields of small to moderate size and varying degrees of alkaline character, including the Flat Tops Wilderness, Elkhead Mountains, and the Yampa volcanic field. These highly alkaline, mafic rocks have been broadly associated with Rio Grande rifting (e.g., Izett, 1975; Larson et al., 1975; Tweto, 1979), and are thought to represent low degrees of partial melting of previously enriched Proterozoic subcontinental mantle lithosphere (Leat et al., 1988, 1989, 1990; Thompson et al., 1990; Beard and Johnson, 1993).

The timing of alkaline volcanism in northwest Colorado related to late Cenozoic extension and Rio Grande rifting is approximately constrained by a few late Miocene to Quaternary K-Ar ages of compositionally diverse rock types (Izett, 1975; Larson et al., 1975; Thompson et al., 1993). Defining a high-precision chronology of this volcanism is essential to establishing any reliable spatial and temporal framework of late Cenozoic extension and volcanism. Because of their highly alkaline character, these rocks favor enrichment of incompatible elements such as the light rare earth elements (LREE) and study of their age and distribution could benefit future mineral exploration.

In this paper we report rock and mineral compositions and $^{40}Ar/^{39}Ar$, Sr, Nd, and Pb isotope data for samples from the volcanic field in and around Yampa, Colorado. These results are the first Pb isotope, $^{40}Ar/^{39}Ar$, and phenocryst compositional data reported from the Yampa volcanic field. Our high-precision $^{40}Ar/^{39}Ar$ geochronology yields Pliocene eruption ages and Pb isotopic data indicating rock derivation from a subcontinental lithospheric mantle that underwent silica-fluid metasomatism ca. 1.74 Ga. Using new and previously published data from northwest Colorado and southern Wyoming we demonstrate that the locus of alkalic volcanism during the past 15 m.y. has migrated toward the Colorado Plateau. We discuss implications of this migrating volcanism and its overall significance to late Cenozoic

Geosphere; April 2014; v. 10; no. 2; p. 374–400; doi:10.1130/GES00921.1; 16 figures; 4 tables.
Received 26 February 2013 ♦ Revision received 9 October 2013 ♦ Accepted 22 January 2014 ♦ Published online 21 February 2014

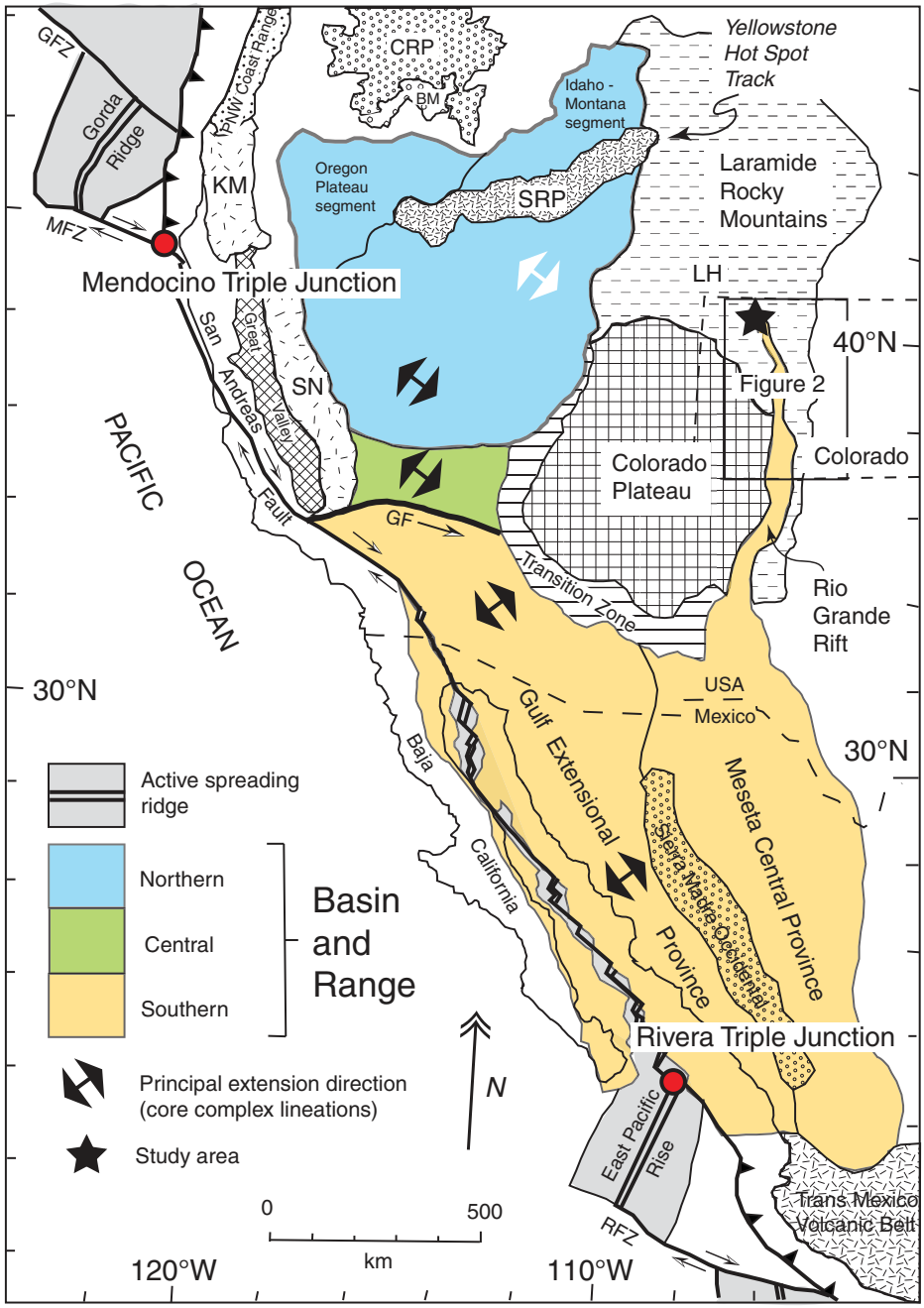

Figure 1. Present-day regional tectonic map of western North America and the Basin and Range province (modified from Dickinson, 2002), with subdivisions of the northern (blue), central (green), and southern (tan) Basin and Range from Jones et al. (1992) and Sonder and Jones (1999). Principal extension directions established from core complex lineations in each region are simplified from Dickinson (2002). White and black arrows indicate areas where core complexes record dominantly Eocene and late Miocene extension, respectively. The dominant northeast-southwest extension in the southern Basin in Range, developed after 20 Ma, records subduction of a transform margin and migration of the Rivera triple junction past Baja California (Lipman et al., 1971; Ingersoll, 1982; Dickinson, 2004). The area of Figure 2 is indicated; star indicates approximate position of Yampa. Abbreviations: BM—Blue Mountains; CRP—Columbia River plateau; GF—Garlock fault; GFZ—Gorda Fracture Zone; KM—Klamath Mountains; LH—Leucite Hills; MFZ—Mendocino Fracture Zone; PNW—Pacific Northwest; RFZ—Rivera Fracture Zone; SN—Sierra Nevada; SRP—Snake River Plain.

extension and the post-Pliocene evolution of the northern Rio Grande rift that includes the Leucite Hills, Wyoming.

NORTHERN RIO GRANDE RIFT

The physiographic Rio Grande rift is marked by a series of discontinuous, sediment-filled grabens, half-grabens, and range-bounding normal faults consisting of three distinctive segments (Chapin, 1979; Ingersoll, 2001). The northernmost segment includes the geomorphic San Luis Valley, a large half-graben fault bounded by the towering (>4000 m elevation) Sangre de Cristo Mountains to the east (Fig. 2). North of the San Luis Valley, the Rio Grande rift is a smaller graben, bounded by the high-elevation Sawatch Range (>4000 m elevation) to the west and the lower elevation Mosquito Range to the east. Immediately north of Leadville is often considered the geographic terminus of the Rio Grande rift, and is where the last semicontinuous rift-like basin bounded by normal faults is exposed. However, block-faulting and downdropped grabens and half-grabens containing late Miocene sediment west of the Gore and Park Ranges and continuing north into Wyoming may represent less conspicuous Rio Grande rifting (Tweto, 1979). The areas between Leadville and the Leucite Hills are herein considered part of the incipient northern Rio Grande rift. Recent uplift of the Rocky Mountain epeirogen (e.g., Eaton, 2008) may obscure unequivocal physiographic expressions of a late Miocene rift-like depression north of Leadville, although an earlier episode of Cenozoic extension is clearly expressed in the North Park, Middle Park, and South Park basins (Fig. 2) that began developing shortly after Laramide arc-style deformation (Cole et al., 2010).

LATE CENOZOIC MANTLE SOURCES OF ALKALINE VOLCANISM IN NORTHWEST COLORADO

Much of the alkaline volcanism bordering the Colorado Plateau in northwest Colorado is associated with northwest-trending extensional fault blocks, and has long been attributed to Rio Grande rifting (Izett, 1975; Larson et al., 1975; Tweto, 1979; Leat et al., 1990, 1991; Beard and Johnson, 1993). The isotopic and chemical composition of their source rocks can provide insight into Rio Grande rifting and also constrain models of interacting asthenospheric and lithospheric mantle in proximity to the Colorado Plateau. For example, recent models show that late Cenozoic volcanic rocks along the southern margins of the Colorado Plateau

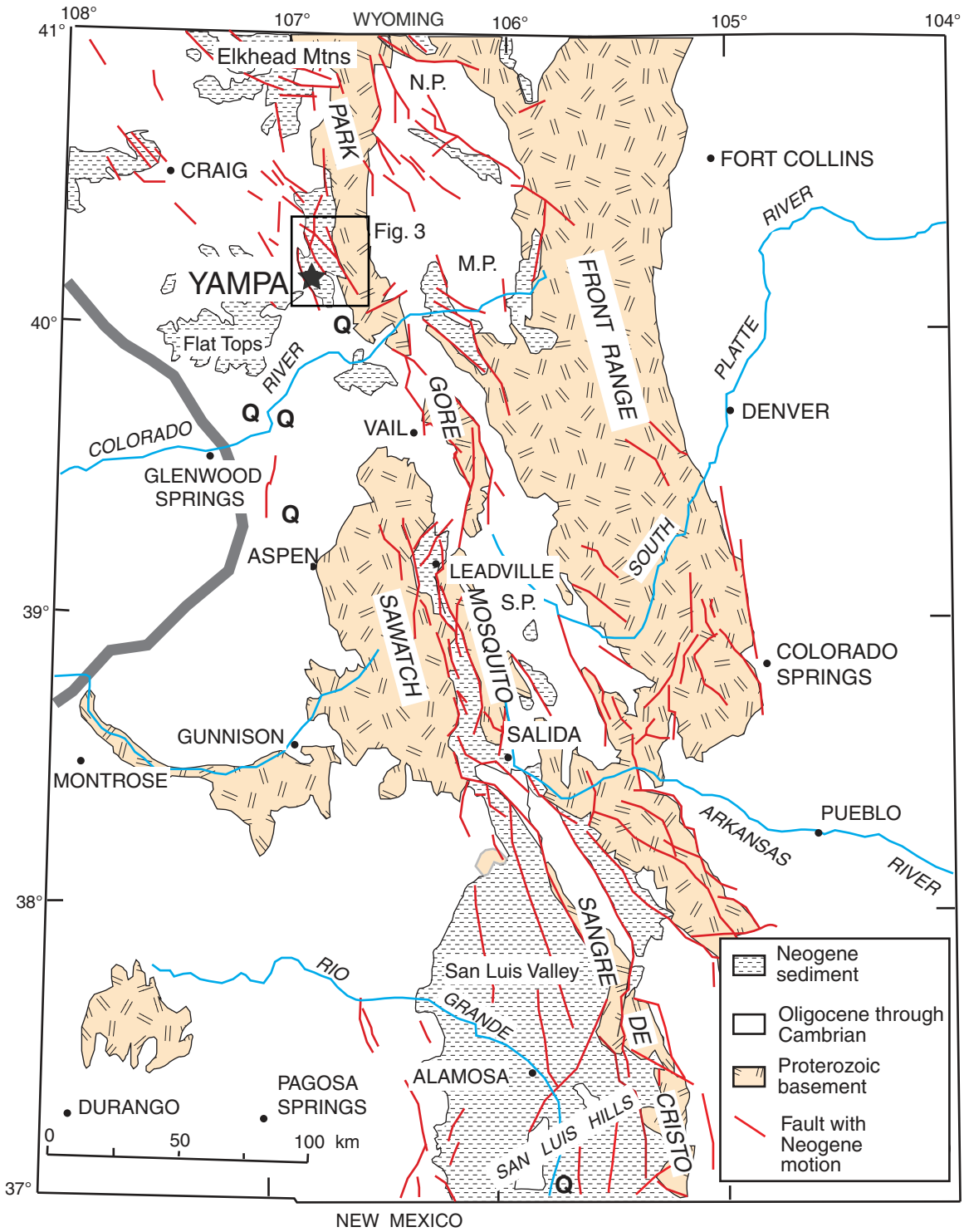

Figure 2. Index map (from Tweto, 1979) of western Colorado highlighting faults with presumed Neogene motion. Thick line is the approximate limit of the Colorado Plateau. The northern limit of the Rio Grande rift is generally drawn just north of Leadville, Colorado, but high-angle block faulting continues into Wyoming along a corridor west of the Gore and Park Ranges, where Miocene and younger volcanic rocks crop out in the Flat Tops Wilderness, the Elkhead Mountains, and near Yampa. Q—known location of Quaternary alkaline lavas. Approximate location of Figure 3 is indicated. N.P.—North Park; M.P.—Middle Park; S.P.—South Park.

become progressively younger and increasingly derived from the asthenospheric mantle approaching the plateau margin, and may reflect large-scale mantle dynamics that control the current size of the plateau, locus of magmatism, and development of relief (e.g., Wenrich et al., 1995; Roy et al., 2009; Crow et al., 2011; Karlstrom et al., 2012).

Both asthenospheric mantle (from Yellowstone) and subcontinental lithospheric mantle sources were proposed by Leat et al. (1991) for lavas from the Yampa volcanic field on the basis of elevated La/Ta ratios and a significant spread in $^{143}Nd/^{144}Nd$ ratios. Beard and Johnson (1993) followed this study by measuring Hf isotopes in lava samples from five separate areas within northwest Colorado sampled by Leat et al. (1988, 1989), including two samples from the Yampa volcanic field. The only samples from northwest Colorado that have $^{176}Hf/^{177}Hf$ isotope data consistent with a continental asthenospheric mantle source are the Yampa lavas, which have $\Delta\varepsilon Hf$ values near zero, overlapping those of the ocean island basalt (OIB) field, and are similar to lavas of the Rio Grande rift near the Colorado–New Mexico border (Beard and Johnson, 1993). Otherwise, all volcanic rocks from northwest Colorado appear restricted to partial melting within the garnet peridotite field, from a subcontinental lithospheric mantle previously enriched by Proterozoic silica-fluid metasomatism within a shallower spinel peridotite field (e.g., Leat et al., 1991; Beard and Johnson, 1993).

AGE CONSTRAINTS ON ALKALINE VOLCANISM IN NORTHWEST COLORADO AND SOUTHERN WYOMING

Fundamental differences in lithospheric thickness beneath the southern and northern Rio Grande rift strongly influence the chemical and isotopic composition of late Cenozoic lavas (e.g., Lipman, 1969; Lipman and Mehnert, 1975; Prodehl and Lipman, 1989; Johnson and Thompson, 1991; Beard and Johnson, 1993; Johnson and Beard, 1993; McMillan et al., 2000), and temporal variations in volcanic rock composition provide important insight into the extent and dynamic evolution of the rift. On the basis of available K-Ar geochronology, Leat et al. (1989) noted three periods of alkaline volcanism in northwest Colorado, the earliest phase represented by Oligocene to early Miocene lamproitic lavas within the Middle Park basin (York et al., 1971; Larson et al., 1975; Thompson et al., 1993, 1997). A second volcanic episode was defined by the late Miocene and Pliocene minettes of the Elkhead Mountains, the Flatops Wilderness, and alkalic lavas near Yampa (Izett, 1975; Larson et al., 1975; Thompson et al., 1993). In the Yampa volcanic field, ages of 7.5–10 Ma were estimated from partially reset fission tracks in apatite separated from basement xenoliths (Izett, 1975) and from two samples with K-Ar ages of 5 and 6 Ma from basalt near Yampa (Thompson et al., 1993). A third volcanic period was noted on the basis of Quaternary mafic volcanic eruptions at Dotsero, McCoy Mountain, Triangle Peak, and Willow Peak (Giegengack, 1962; Larson et al., 1975; Leat et al., 1990). Lange et al. (2000) reported high-precision $^{40}Ar/^{39}Ar$ ages between 0.9 and 1.3 Ma for the highly alkalic rocks of the Leucite Hills (Carmichael, 1967), and it is the only volcanic field along the northeast margin of the Colorado Plateau characterized by high-precision $^{40}Ar/^{39}Ar$ geochronology. Establishing a similarly precise chronology of the eruptive sequences in northwest Colorado is necessary before rigorous testing of any models incorporating temporal constraints.

METHODS

Samples

Samples of fresh, xenolith-free, volcanic rock were examined petrographically using polarizing and scanning electron microscopes, analyzed chemically by electron microprobe, and aliquots were prepared for geochemistry, $^{40}Ar/^{39}Ar$ geochronology, and Sr, Nd, and Pb isotope analysis. We sampled volcanic rock at six representative sites near Yampa, where numerous small volcanic necks, dikes, and lava flows occur as part of a small volcanic field west of the Park Range near Yampa (Fig. 3). Most of the volcanic rocks occur within or along the margins of small grabens and half-grabens containing sediment of the Miocene Browns Park Formation (Fig. 4). The lavas were forcibly emplaced, and most contain numerous shallow crustal xenoliths of the Browns Park Formation, ranging in diameter from a few millimeters to several meters, but also include centimeter-sized

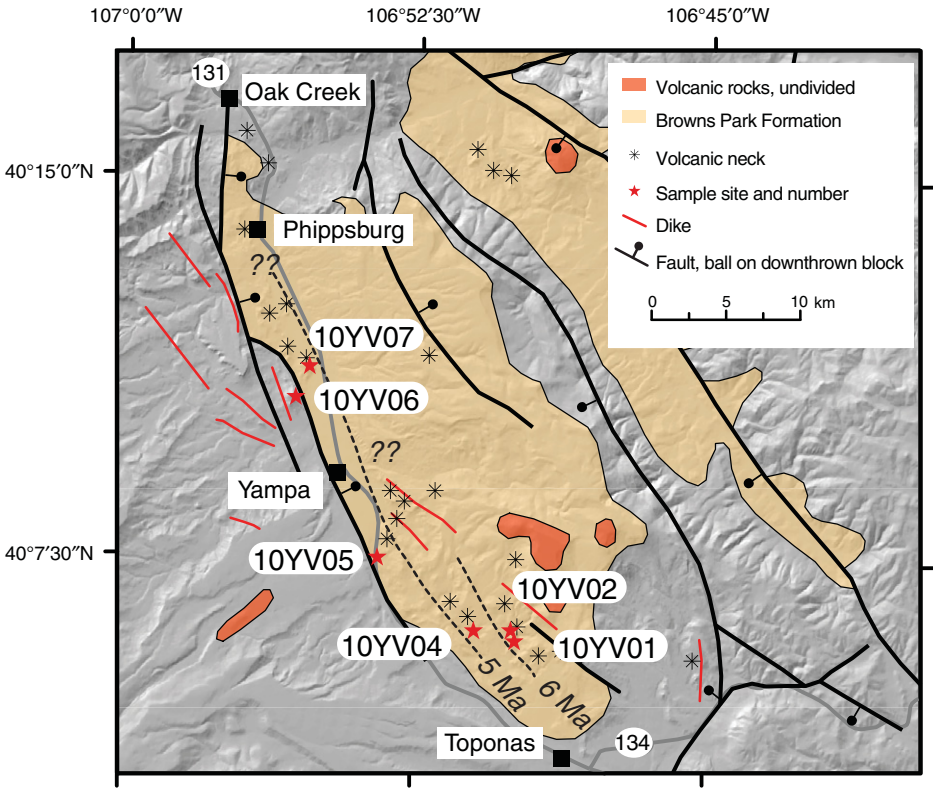

Figure 3. Sample localities from this study plotted on a shaded relief map of the Yampa region overlain with simplified geology, normal faults, and volcanic necks and dikes (from Tweto, 1979). Note the position of volcanic necks relative to high-angle normal faults bounding half-grabens filled by the Miocene Browns Park Formation. Also shown are undifferentiated volcanic rocks of presumed Miocene age. Dashed lines delineate migrating zones of contemporaneous volcanic activity based upon $^{40}Ar/^{39}Ar$ data from this study.

xenoliths of Precambrian basement rocks (Leat and Thompson, 1988) (Fig. 5).

Petrography

The Yampa lavas have millimeter-sized phenocrysts of olivine and clinopyroxene and minor Ti-phlogopite and orthopyroxene in a vesiculated groundmass of plagioclase, clinopyroxene, iron oxides, and glass (Fig. 6). Olivine forms both tabular and skeletal crystals and the largest phenocrysts have been significantly replaced by chlorite. The larger clinopyroxene phenocrysts contain melt pools in their cores and have rims with numerous fine-scale, compositionally distinct bands, as indicated by petrographic observation (Fig. 6) and backscattered electron imaging (Fig. 7). The prominent sieve texture preserved in many of the larger olivine and clinopyroxene phenocrysts (Fig. 7) suggests that they are melting and that the fine-scale zoning of the rims is tracking chemical equilibrium with a melt phase during crystal growth. Vesicles observed in many samples contain secondary calcite.

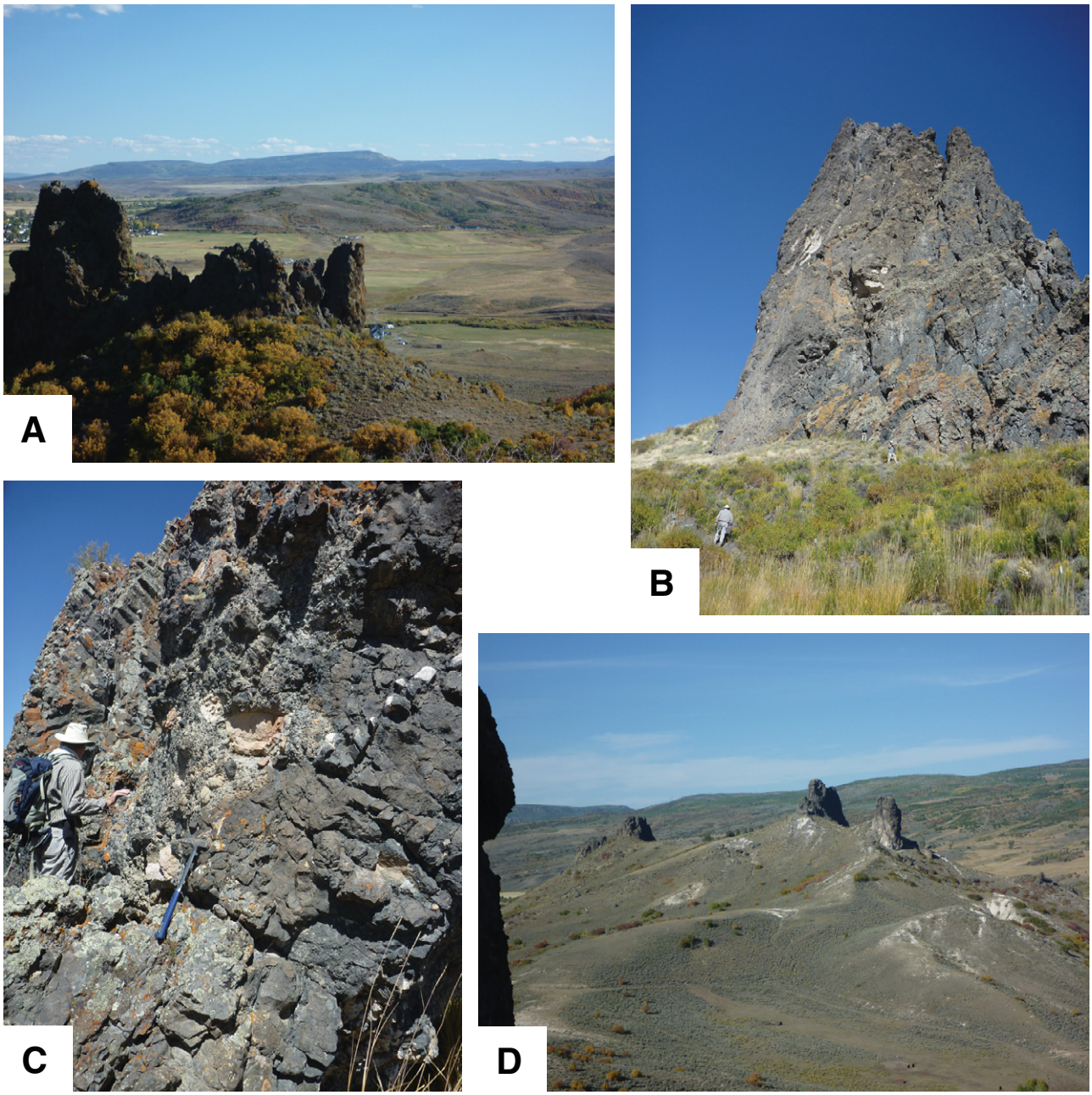

Figure 4. Photographs illustrating occurrence of volcanic rocks of the Yampa area. (A) View to east of locality 10YV-07, a volcanic dike near Yampa. Note the low relief defined by northwest-southeast–trending normal faults bounding half-grabens. (B) Locality 10YV-05, a typical volcanic neck observed in the Yampa area. (C) Closeup view of volcanic neck at locality 10YV-01, illustrating subvertical flow-banding in volcanic neck. (D) View of northwest-southeast–trending volcanic dike intruding the Miocene Browns Park Formation taken from locality 10YV-07, looking toward the northeast.

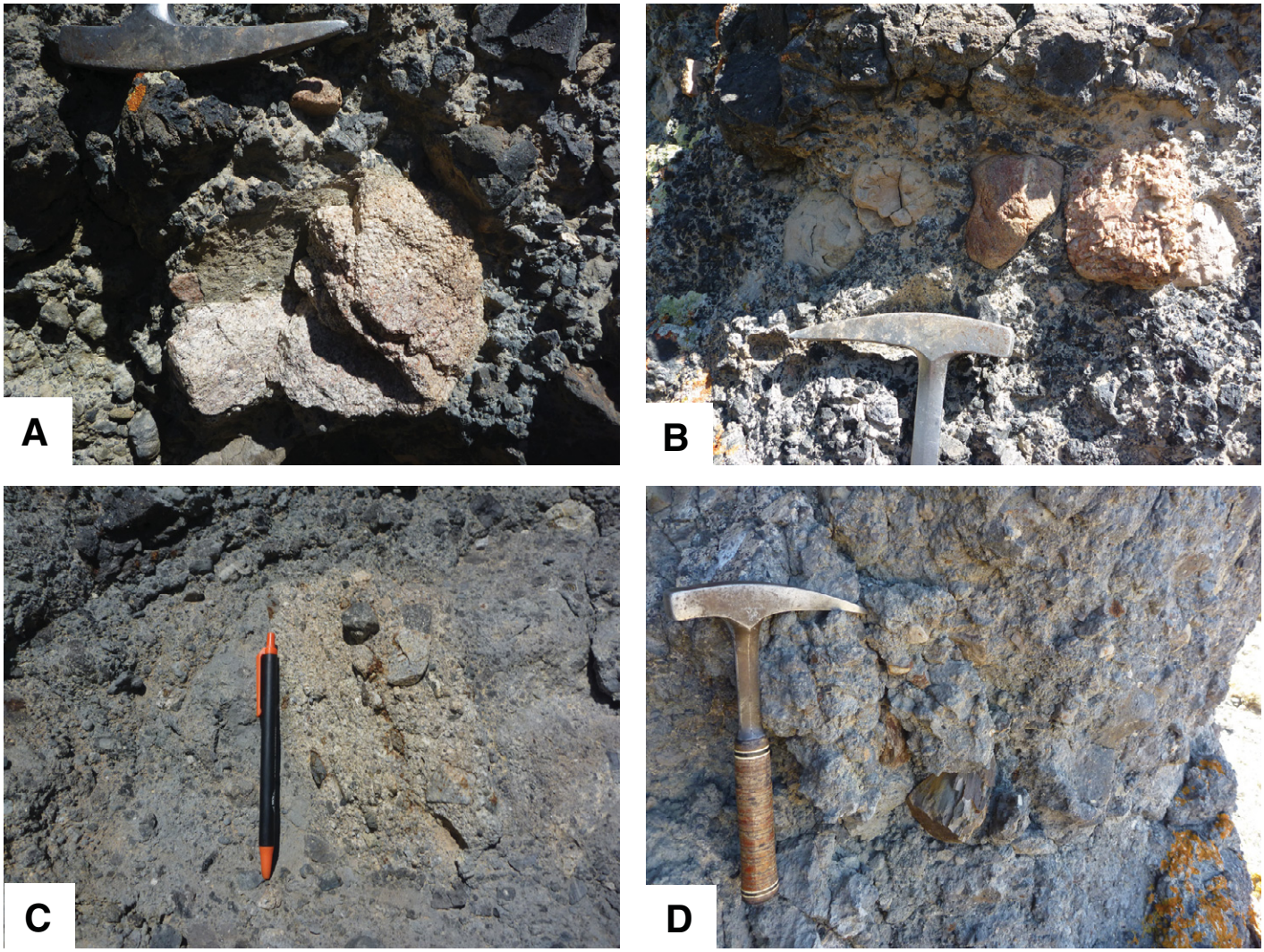

Figure 5. (A–D) Crustal xenoliths are observed in volcanic rock from different outcrops of the Yampa area, including gneiss, conglomerate, and siltstone.

Rock Compositions

Major and minor element concentrations were determined at the U.S. Geological Survey (USGS) in Denver on rock powders by quantitative X-ray fluorescence spectrometry, and trace element concentrations (including REEs) were determined by inductively coupled plasma mass spectrometry. For the trace element analyses, the whole-rock powders were digested overnight on a hot plate; external precisions of the reported trace element concentrations are ~10% based on replicate analyses of the BCR-1 USGS standard.

Sr, Nd, and Pb Isotopes

The analytical techniques used for simultaneous, single-dissolution of U-Th-Pb, Rb-Sr, and Sm-Nd analysis on whole rocks for this study are similar to those reported in more detail by Tatsumoto and Unruh (1976), and Premo and Loucks (2000). Whole-rock samples were dissolved in 7 mL Teflon PFA vials with ultrapure concentrated HF + HNO_3 and then spiked with a dilute mixed tracer of ^{205}Pb-^{233}U-^{236}U-^{230}Th as well as dilute mixed tracers of ^{84}Sr-^{87}Rb and ^{150}Nd-^{149}Sm. Samples were reheated to achieve isotopic equilibration. Lead was extracted using AG 1-X8 anion exchange resin in Teflon microcolumns using a very dilute HBr medium. Lead residues were dried in H_3PO_4 and loaded onto single Re filaments. The Pb laboratory contamination (blank) varied between 50 and 110 pg total Pb (average = 67 ± 8 pg), and had a measured composition of $^{206}Pb/^{204}Pb$ = 18.681 ± 0.064, $^{207}Pb/^{204}Pb$ = 15.432 ± 0.033, and $^{208}Pb/^{204}Pb$ = 37.720 ± 0.120 from multiple determinations. Uranium and Th were then extracted from the Pb eluent using AG 1-X8 anion exchange resin in a different, slightly larger, Teflon microcolumn using a 7N HNO_3 medium, and residues were loaded onto Re filaments using dilute HNO_3. Uranium blank levels were 15–25 pg, and Th blank levels were 1–6 pg. The effluent was then passed through a large (30 mL resin volume) column with AG 50W-X8 cation exchange resin, separating Rb, Sr, and the REEs. Strontium and Rb were further purified using a smaller Teflon column with AG 50W-X8 cation exchange resin; Sr was dried in H_3PO_4 acid and run on a single oxidized Ta filament, and Rb was run in a double rhenium filament configuration. Laboratory contamination levels of total Sr typically range between 30 and 300 pg. Rubidium blanks were typically

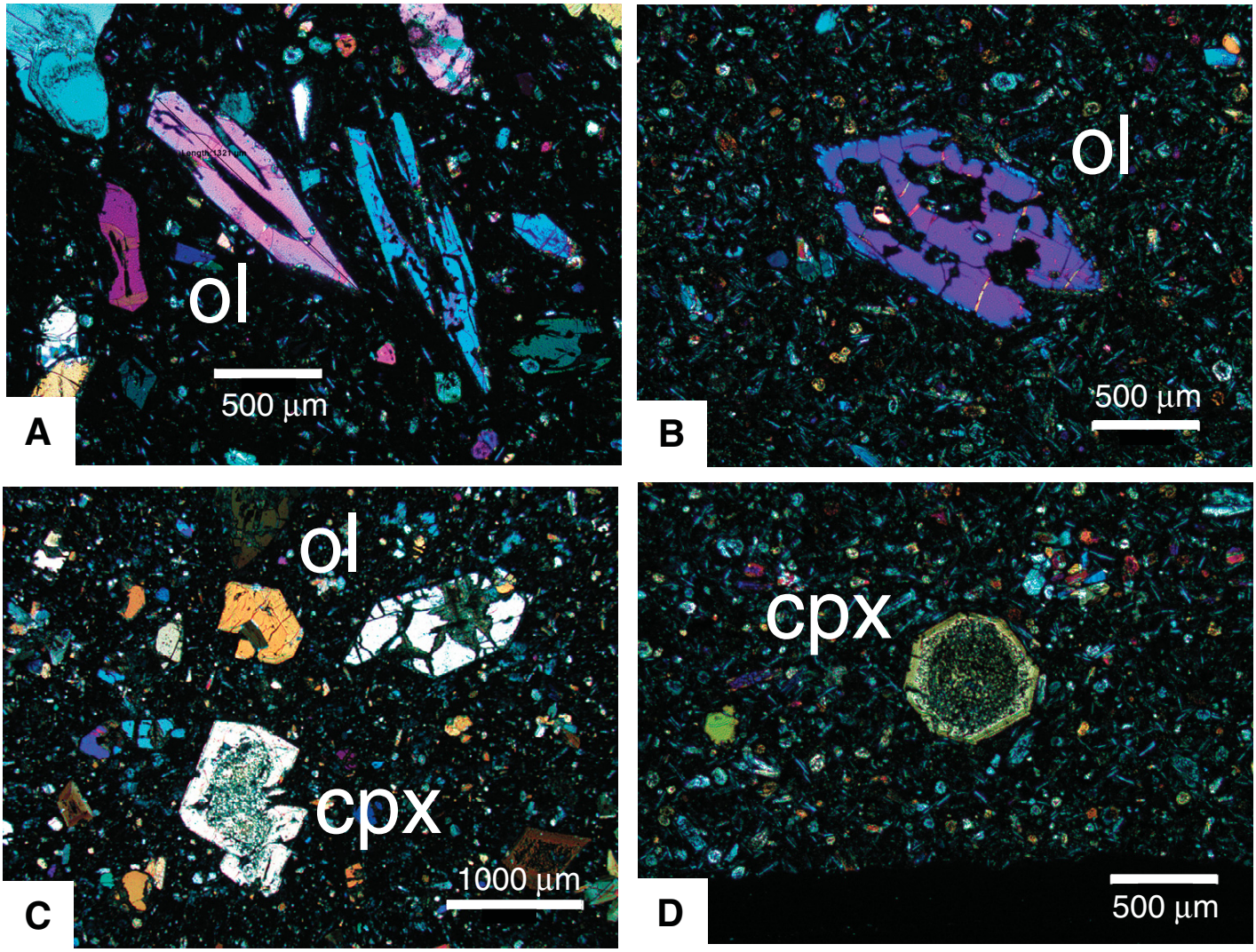

Figure 6. Photographs of Yampa thin sections. (A) Sample 10YV-07, skeletal olivine (ol) phenocrysts in fine-grained, glassy matrix. (B) Sample 10YV-05, partially resorbed, tabular and zoned olivine phenocryst in fine-grained glassy matrix. (C) Sample 10YV-02, tabular olivine phenocrysts and clinopyroxene (cpx) phenocrysts with partially melted cores. (D) Sample 10YV-05, end sectional view of clinopyroxene phenocryst with a partially melted core and rim precipitated from a melt.

five times smaller than those for Sr. Samarium was separated from Nd using AG 50W-X8 cation exchange resin and the α-isobutyric method of Lugmair et al. (1975), cleaned further using smaller Teflon columns with AG 50W-X8 cation exchange resin, then loaded with very dilute H_3PO_4 acid onto triple Ta filaments. Laboratory contamination levels of total Nd were between 30 and 250 pg; samarium blanks were typically 3–5 times smaller than those for Nd.

The Pb isotopes were measured using a Triton multicollector thermal ionization mass spectrometer (TIMS) in static mode using Faraday cups. The Pb isotope ratios were corrected for mass discrimination of 0.0010 ± 0.0003 per mass unit using data for National Institute of Standards and Technology (NIST) standards SRM-981 and SRM-982 measured at the same run conditions. The external uncertainty of the standard analyses was mainly due to mass fractionation effects, and was 0.08%, 0.12%, and 0.16% for $^{206}Pb/^{204}Pb$, $^{207}Pb/^{204}Pb$, and $^{208}Pb/^{204}Pb$, respectively. The concentrations and isotopic ratios of U, Th, Rb, Sr, Sm, and Nd were determined on an automated, multisample, single-collector, VG Isomass 54R TIMS using the ANALYST programming of Ludwig (1992). Typical runs per element varied with desired level of precision, but for both Sr and Nd, a minimum of 240 measurements were collected to achieve a 0.003% error. Concentration uncertainties vary between ~0.1% and ~1.0%. All isotopic ratios were corrected for blank and instrumental mass fractionation, $^{87}Sr/^{86}Sr$ data were normalized to $^{86}Sr/^{88}Sr = 0.1194$, and monitored for instrumental bias using the NIST SRM 987 standard; the mean value of $^{87}Sr/^{86}Sr$ for 30 analyses of the Sr standard during the course of this study was 0.710265 ± 10 (2σ). The $^{143}Nd/^{144}Nd$ data were normalized to $^{146}Nd/^{144}Nd = 0.7219$ and monitored for instrumental bias using the La Jolla Nd standard, which yielded a mean value of $^{143}Nd/^{144}Nd = 0.511865 \pm 10$ (2σ) for 30 replicate analyses. The initial $^{87}Sr/^{86}Sr$ and $^{143}Nd/^{144}Nd$ values were calculated using measured Rb/Sr, Sm/Nd, and $^{40}Ar/^{39}Ar$ ages for the same samples. The $\varepsilon_{Nd}(0)$ values were calculated using present-day $(^{143}Nd/^{144}Nd)_{CHUR} = 0.512636$, and $(^{147}Sm/^{144}Nd)_{CHUR} = 0.1967$ (CHUR is chondritic uniform reservoir).

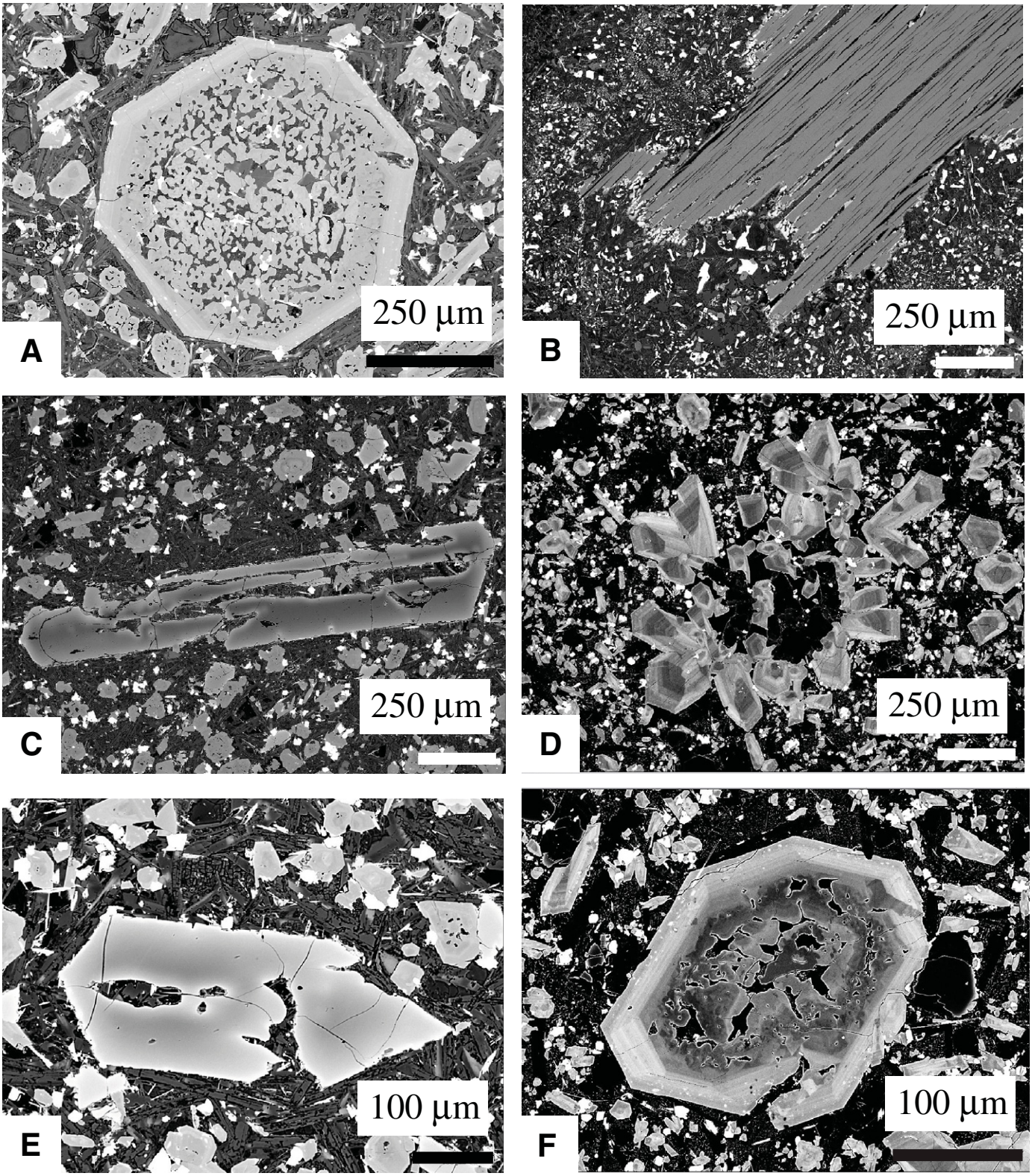

Figure 7. Backscattered electron images of Yampa samples. (A) Sample 10YV-05, zoned clinopyroxene phenocryst with a core displaying evidence of melting, and a rim with growth zones formed during precipitation from a melt. (B) Sample 10YV-04a, relict Ti-phlogopite phenocryst partially decomposed within a fine-grained glassy matrix. (C) Sample 10YV-04a, skeletal olivine with smaller olivine in a fine-grained glassy groundmass. (D) Sample 10YV-02, cluster of compositionally zoned clinopyroxene centered around a glassy pseudomorph of a once-stable clinopyroxene. (E) Sample 10YV-04a, zoned olivine phenocryst. (F) Sample 10YV-02, zoned clinopyroxene phenocryst with melting core and finely banded rims precipitated during ascent prior to eruption.

$^{40}Ar/^{39}Ar$ Geochronology

The $^{40}Ar/^{39}Ar$ analyses were performed at the USGS in Denver, Colorado. Samples were prepared by crushing and isolating rock fragments of ~1 mm^3 from fresh rock free of obvious alteration and xenocrysts. The rock fragments were washed in deionized water and together with standards, were irradiated for 20 MW hours in the central thimble position of the USGS TRIGA reactor. Laser fusion of >10 individual Fish Canyon Tuff sanidine crystals (28.20 ± 0.09 Ma; Kuiper et al., 2008) at each closely monitored position within the irradiation package resulted in neutron flux ratios reproducible to ±0.25% (2σ). Isotopic production ratios and interfering nucleogenic reactions were determined from irradiated CaF_2 and KCl salts and zero age K-silicate glass, and for this study the following values were measured: $(^{36}Ar/^{37}Ar)_{Ca}$ = (2.77 ± 0.03) × 10^{-4}; $(^{39}Ar/^{37}Ar)_{Ca}$ = (6.54 ± 0.33) × 10^{-4}; and $(^{38}Ar/^{39}Ar)_{K}$ = (1.29 ± 0.03) × 10^{-2}. Cadmium shielding during irradiation prevented any measurable nucleogenic $(^{40}Ar/^{39}Ar)_{K}$. The irradiated basalt samples and standards were loaded into numbered positions of a stainless steel planchette, placed into a laser sample chamber with an externally pumped ZnSe window, and evacuated to ultrahigh vacuum conditions in a fully automated stainless steel extraction line designed and built at the USGS in Denver. Using a 25W CO_2 laser equipped with a beam homogenizing lens, the samples were incrementally heated and the liberated gas was expanded and purified by exposure to a cryogenic trap maintained at −140 ºC and two hot SAES GP50 getters. Following purification the gas was expanded online into a Mass Analyzer Products 215–50 mass spectrometer in static mode and Ar isotopes were measured by peak jumping using an electron multiplier in analog mode. Data were acquired during 10 measurement cycles and time zero intercepts were determined by best-fit linear and/or polynomial regressions to the data. Data were corrected for mass discrimination, blanks, radioactive decay, and interfering nucleogenic reactions.

TABLE 1. WHOLE-ROCK MAJOR AND TRACE ELEMENT DATA OF YAMPA LAVAS

Sample,	10YV01A	10YV02A	10YV04A	10YV04B	10YV05	10YV06	10YV07
rock type	basanite	basanite	trachybasalt	trachybasalt	trachybasalt	basalt	trachybasalt
SiO_2	43.19	41.66	47.20	47.36	46.64	47.39	45.03
TiO_2	2.16	2.12	2.10	2.18	1.80	1.91	2.17
Al_2O_3	13.68	13.03	14.36	14.38	14.24	14.42	13.82
Fe_2O_3	11.58	11.08	9.77	10.03	9.87	11.35	9.79
FeO							
MnO	0.17	0.18	0.16	0.16	0.16	0.14	0.16
MgO	9.73	9.74	7.03	7.12	7.89	4.72	8.27
CaO	10.37	11.32	8.38	8.52	9.34	10.37	10.80
Na_2O	2.77	1.48	3.23	3.42	3.60	2.83	2.76
K_2O	2.14	2.54	3.39	3.28	2.93	1.60	2.72
P_2O_5	1.03	1.03	0.82	0.83	0.90	0.91	0.85
LOI	1.63	3.39	2.48	2.40	1.43	2.80	1.52
Sum	98.45	97.55	98.91	99.68	98.80	98.43	97.88
Cr	247	251	125	141	176	220	184
Ni	166	168	118	122	140	104	141
S	101	621	267	130	140	86	362
Sc	38	41	35	35	35	42	43
V	214	218	183	186	195	215	203
Co	50	48	39	42	42	43	43
Cu	51	39	32	39	34	35	58
Zn	95	94	101	99	97	103	86
Ga	18	17	20	18	18	17	17
Ge	10	6	8	9	9	8	8
Br	1	0	0	0	0	1	1
Rb	35	39	60	62	58	28	52
Sr	1318	1787	1276	1104	1523	1164	1030
Y	24	24	24	24	25	22	25
Zr	281	264	304	274	296	203	255
Nb	63	59	84	83	71	32	70
Sb	4	3	2	0	3	2	4
Ba	1694	1752	1390	1330	1855	922	1260
As	0	1	0	1	2	3	1
La	71	69	63	66	75	49	64
Ce	143	141	121	127	145	107	127
Pr	17	17	14	15	17	14	15
Nd	67	65	54	56	65	58	57
Sm	11	11	10	10	11	10	10
Eu	3	3	3	3	3	3	3
Tb	1	1	1	1	1	1	1
Gd	9	9	8	8	9	8	9
Dy	6	6	6	6	6	5	6
Ho	1	1	1	1	1	1	1
Er	3	3	3	3	3	2	3
Tm	0	0	0	0	0	0	0
Yb	2	2	2	2	2	2	2
Lu	0	0	0	0	0	0	0
W	<7	<7	<7	<7	<7	<7	<7
Tl	<3	<3	<3	<3	<3	<3	<3
Pb	9	11	11	20	12	7	11
Th	7	7	8	8	8	4	13
U	2	2	3	3	2	1	2

Note: Major elements are in weight percent and trace element data are in parts per million. LOI—loss on ignition.

RESULTS

Rock Compositions

The Yampa volcanic rocks collected for this study are mafic (SiO_2 = 41.5–47.5 wt%; MgO = 5–10 wt%), and alkalic ($Na_2O + K_2O$ = 4–7 wt%), with high TiO_2 (1.8–2.2 wt%) and P_2O_5 (0.8–1.0 wt%) (Table 1). These rocks plot as basanites, trachybasalts, and basalt with normative nepheline contents to 20% (Fig. 8) and have compositions similar to those reported in Leat et al. (1991). The Yampa lavas show slight positive correlations of Al_2O_3 with SiO_2, whereas MgO and CaO are inversely correlated (Fig. 9A), indicating variable modal phenocryst abundances of olivine, clinopyroxene, and plagioclase relative to groundmass. Plots of TiO_2 versus the other oxides (Fig. 9B), useful in evaluating geochemistry of high-Ti alkaline lavas (e.g., Carmichael et al., 1996), show that Ti is positively correlated with Nb (Fig. 10), consistent with a rutile-bearing source region (e.g., Foley et al., 2000). Elevated P_2O_5 contents support a P-rich source, possibly including apatite, and the metastable Ti-phlogopite preserved in sample 10YV-04A is a possible mantle source for the high Ti, Ba, and

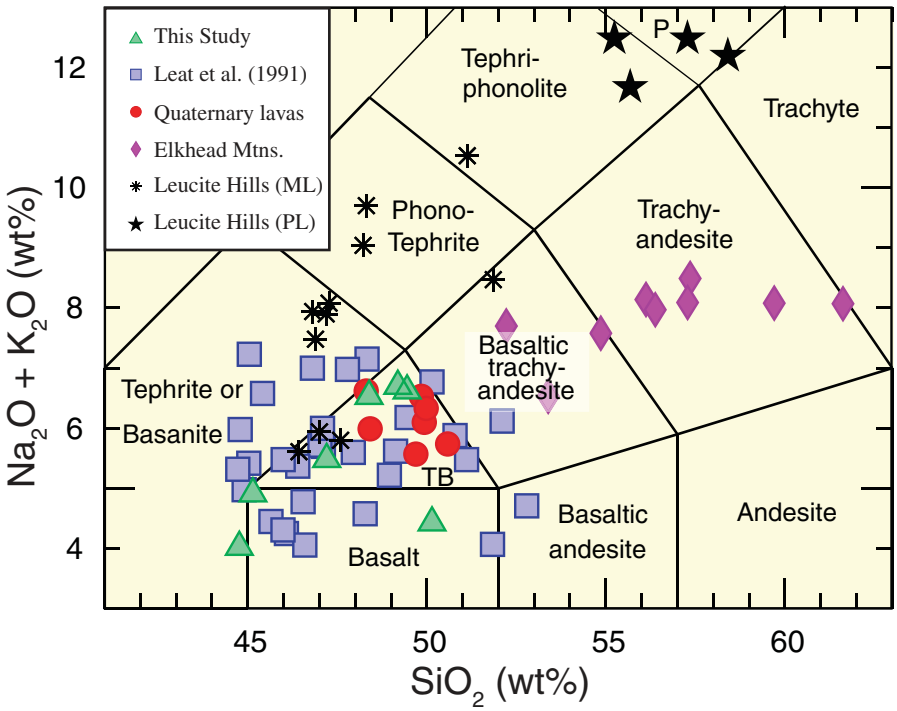

Figure 8. Whole-rock compositions from this study together with data from Leat et al. (1991) plotted on the discrimination diagram of Le Maitre et al. (1989). TB—trachybasalt; P—phonolite. Sources of data: triangles—Yampa lavas from this study; squares—Yampa lavas from Leat et al. (1991); circles—Quaternary basalts from Leat et al. (1989); diamonds—minettes of the Elkhead Mountains; Thompson et al. (1990); stars—phlogopite lamproite (PL) and asterisks—madupite lamproite (ML) of the Leucite Hills (Mirnejad and Bell, 2006).

Rb concentrations (e.g., Schmidt et al., 1999) in these rocks.

The trace element composition of the Yampa samples have moderately elevated large ion lithophile element relative to OIB and highly enriched LREE concentrations relative to chondrites (Fig. 10). These new results are generally similar to those from early Miocene minettes from the Elkhead Mountains (Thompson et al., 1990) and the Quaternary alkaline basalts of northern Colorado (Leat et al., 1989), and slightly less enriched than the lamproites of the Leucite Hills (Mirnejad and Bell, 2006) (Fig. 10). Although the Yampa samples have elevated Rb/Nb, Ti/Nb, and La/Nb ratios relative to OIB, they plot on trajectories toward even higher ratios characteristic of some highly silicic minettes in the Elkhead Mountains (Fig. 10).

Mineral Compositions

Compositions of olivine, clinopyroxene, and phlogopite phenocrysts were determined from electron microprobe analyses, and both olivine and clinopyroxene phenocrysts exhibit significant compositional zoning (Table 2). Olivines have systematically Mg- and Ni-enriched cores and Fe- and Ca-enriched rims (Table 2; Fig. 11). Polarized light and backscattered electron imaging of compositional zoning in clinopyroxene phenocrysts (Figs. 6 and 7) is confirmed by the electron microprobe data, which show uniform enrichments in Si, Fe^{2+}, and Na in cores indicating a small, but significant jadeite component (Table 2), and rims with marked enrichments of Ca, Mg, Al, and Ti relative to phenocryst cores. The clinopyroxene core and rim compositions require the following cation exchanges: Si ⇔ Ti, Fe ⇔ Mg, and NaSi ⇔ CaAl. Two quantitative microprobe traverses across one large (3 mm) phenocryst from sample 10YV-02 are representative of compositional variations observed among all analyzed samples (Fig. 12), with uniform compositions in the surviving clinopyroxene core and fine-scale, compositionally distinct bands along its rims.

Sr, Nd, and Pb Isotopes

The $^{206}Pb/^{204}Pb$ (17.5–18), and $^{208}Pb/^{204}Pb$ (37.3–37.6) ratios of the Yampa lavas (Table 3) are similar to Pb isotope data from numerous mafic, intermediate, and felsic basement samples of the Green Mountain arc terrane (Fig. 13A), a Proterozoic subduction zone or volcanic arc complex extending from northern Colorado to southwestern Wyoming (Hills and Houston, 1979; Premo and Loucks, 2000; Jones et al., 2011b). The high-grade metamorphic basement rocks of the Green Mountain arc terrane plot below the terrestrial Pb (bulk silicate Earth) evolution model of Stacey and Kramers (1975), consistent with time-integrated, hybrid mantle sources, and define a poorly constrained whole-rock Pb-Pb age of 1743 ± 64 Ma (mean square of weighted deviates, MSWD = 14), identical to U-Pb zircon ages from the regional basement rocks (Premo and Van Schmus, 1989). The Yampa lavas taken alone define a poorly constrained Pb-Pb age of 1998 ± 210 Ma (Fig. 13B), with Pb isotope values shared by mafic lower crust in this area, consistent with some lower crustal assimilation. Given the abundance of crustal xenoliths observed in the Yampa lavas, including sediments of the Miocene Browns Park Formation and high-grade gneisses, some degree of crustal assimilation seems unavoidable, yet the low $^{207}Pb/^{204}Pb$ (and $^{87}Sr/^{86}Sr$) ratios suggest little upper crustal assimilation in these lavas.

The $^{143}Nd/^{144}Nd$ values of Yampa lavas range from 0.512327 to 0.512553 [$\varepsilon_{Nd}(0)$ values of 0 to −7] and initial $^{87}Sr/^{86}Sr$ values of 0.704–0.706 (Table 3), similar to those previously identified from other Yampa lavas (Leat et al., 1988). The Yampa lavas have a cumulative difference in radiogenic Nd of ~7 ε_{Nd} units, but no clearly defined trend in $^{87}Sr/^{86}Sr$ (Fig. 14A). This range in $^{143}Nd/^{144}Nd$ and $^{87}Sr/^{86}Sr$ ratios is consistent with melting some component of mafic basement of the Green Mountain arc terrane (Fig. 14B), and the range of ε_{Nd} and Δ_{Hf} values also suggests a possible component of asthenospheric mantle (e.g., Leat et al., 1988; Beard and Johnson, 1993). A similar range in ε_{Nd} values and restricted $^{87}Sr/^{86}Sr$ ratios is observed in the Elkhead Mountains, Yarmony Mountain, and younger Quaternary basalts from northern Colorado (Fig. 14B), but compared to the Yampa lavas their more negative ε_{Nd} and Δ_{Hf} values indicate source regions restricted to the subcontinental lithospheric mantle (Beard and Johnson, 1993).

$^{40}Ar/^{39}Ar$ Geochronology

Results of the Yampa whole-rock $^{40}Ar/^{39}Ar$ incremental CO_2-laser heating experiments are presented in Table 4, and $^{40}Ar/^{39}Ar$ age spectra and $^{39}Ar/^{40}Ar$ versus $^{36}Ar/^{40}Ar$ isochrons are plotted in Figure 15; samples 10YV-01A and 10YV-01B were taken from different parts of one outcrop, and duplicate analyses of samples 10YV-02 and 10YV-05 are also shown. The

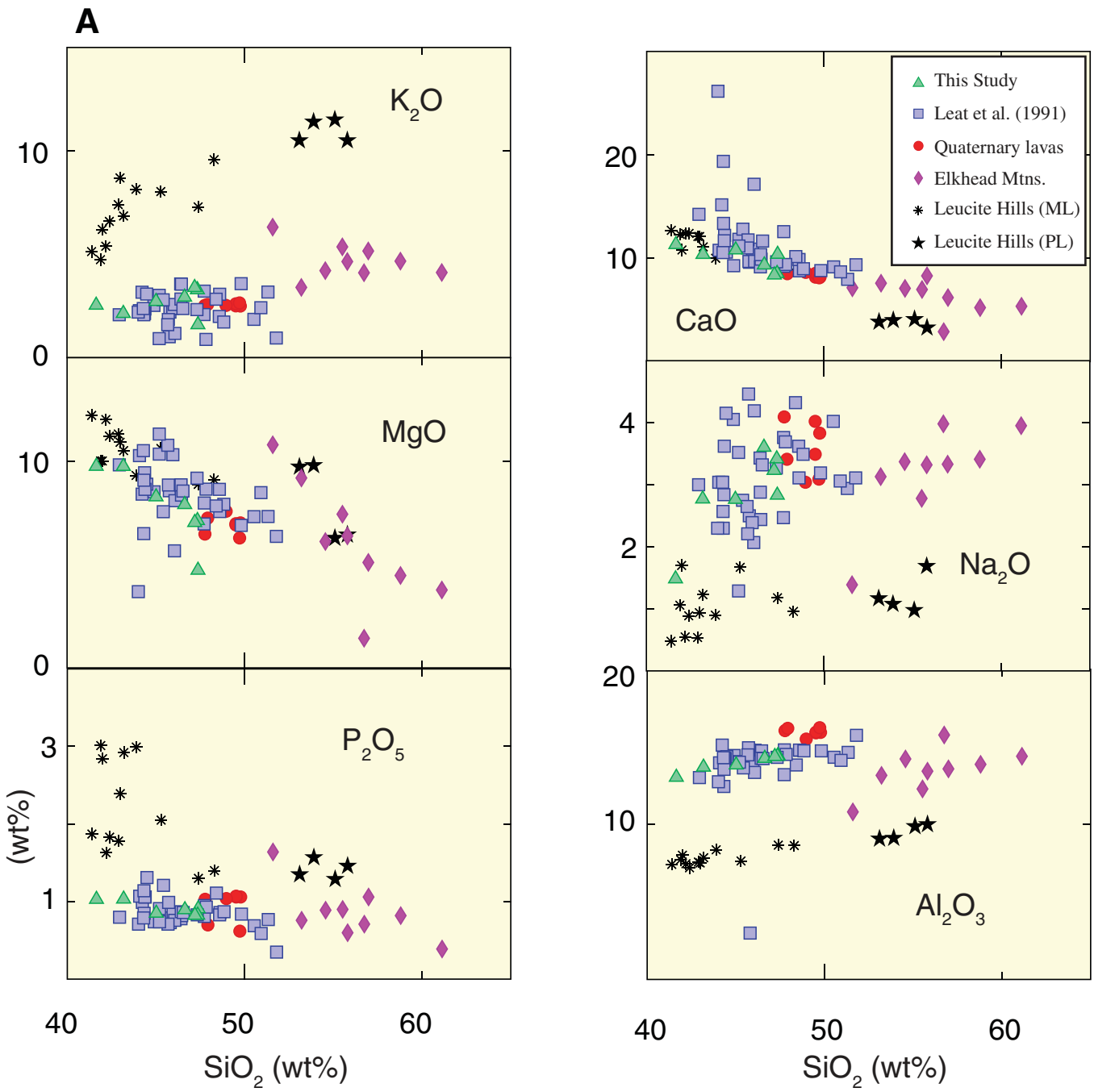

Figure 9 (*Continued on following page*). (A) Plots of selected major element oxide compositions versus SiO_2 (wt%).

$^{39}Ar/^{40}Ar$ versus $^{36}Ar/^{40}Ar$ isochrons for the Yampa samples (Fig. 15A) indicate trapped argon with $^{40}Ar/^{36}Ar$ values (ordinate intercept) significantly higher than the present atmospheric value of 298.56 (Lee et al., 2006). Excepting sample 10YV-06 (with insufficient isotopic differences between incremental heating steps to calculate a statistically valid isochron), samples plot along isochrons (MSWD < 2) with ages between 6.0 ± 0.3 Ma (10YV-01B) and 4.47 ± 0.11 Ma (10YV-05B) and have trapped $^{40}Ar/^{36}Ar$ ratios >300. The $^{40}Ar/^{39}Ar$ age spectra calculated assuming atmospheric $^{40}Ar/^{36}Ar$ values (298.56) for trapped argon are irregular (Fig. 15B) and lack $^{40}Ar/^{39}Ar$ plateau ages (3 or more consecutive heating steps with statistically identical [2σ] ages and combined total more than 50% of the cumulative ^{39}Ar released). Only one sample (10YV-04B) has trapped $^{40}Ar/^{36}Ar$ ratios within error of present-day atmosphere, and has identical errorchron (5.04 ± 0.11 Ma) and near-plateau (5.06 ± 0.5 Ma) ages (Figs. 15A, 15B). Replotting all of the $^{40}Ar/^{39}Ar$ age spectra with the isochron-defined $^{40}Ar/^{36}Ar$ ratios (Fig. 15C) results in age spectra with $^{40}Ar/^{39}Ar$ age plateaus for nearly all samples with ages ranging between 6.08 ± 0.06 Ma (10YV-02A) and 4.59 ± 0.05 Ma (10YV-05A). Because the Yampa lavas have isochrons that indicate mixing with some extraneous argon

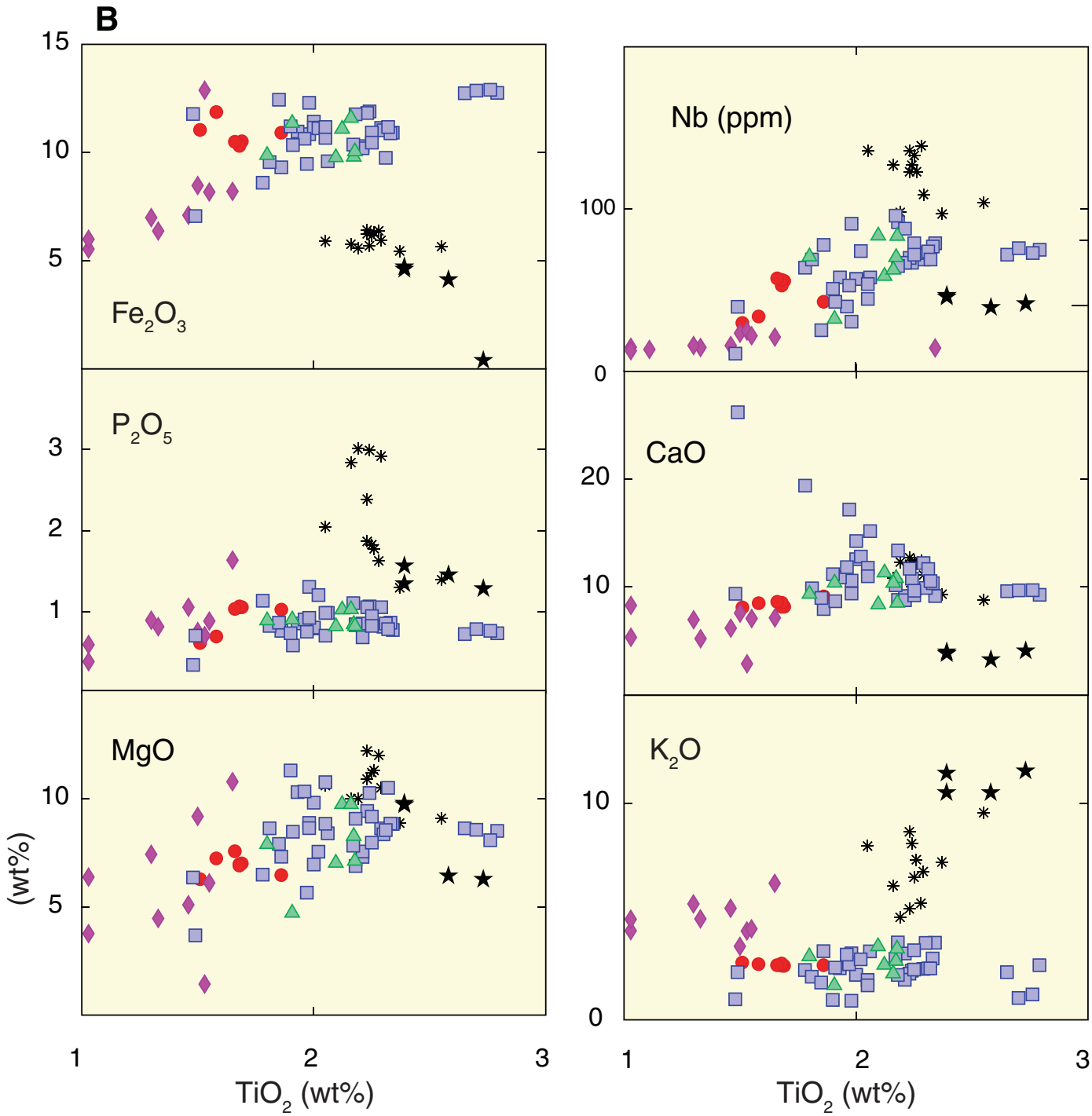

Figure 9 (*Continued*). (B) Plots of selected major element oxide compositions versus TiO_2 (wt%). Sources of data as in Figure 8. PL—phlogopite lamproite; ML—madupite lamproite.

with nonatmospheric $^{40}Ar/^{36}Ar$ values, the isochrons or age spectra using the isochron-derived trapped argon values most accurately define eruption ages within the Yampa volcanic field. The source of the extraneous argon may be related to assimilation of xenoliths of crustal rock prior to or during eruption. Sample 10YV06, with an integrated age of 22.5 ± 0.6 Ma, is the only true basalt sampled and contains half the magnesium of the other samples and is the only sample in which relict orthopyroxene was identified. Further work is required to determine the geochronological and geological significance of this sample.

DISCUSSION

Phenocryst Zoning and the Transition from Lithospheric Mantle to the Surface

Despite numerous crustal xenoliths contained in the Yampa volcanic rocks, no ultramafic

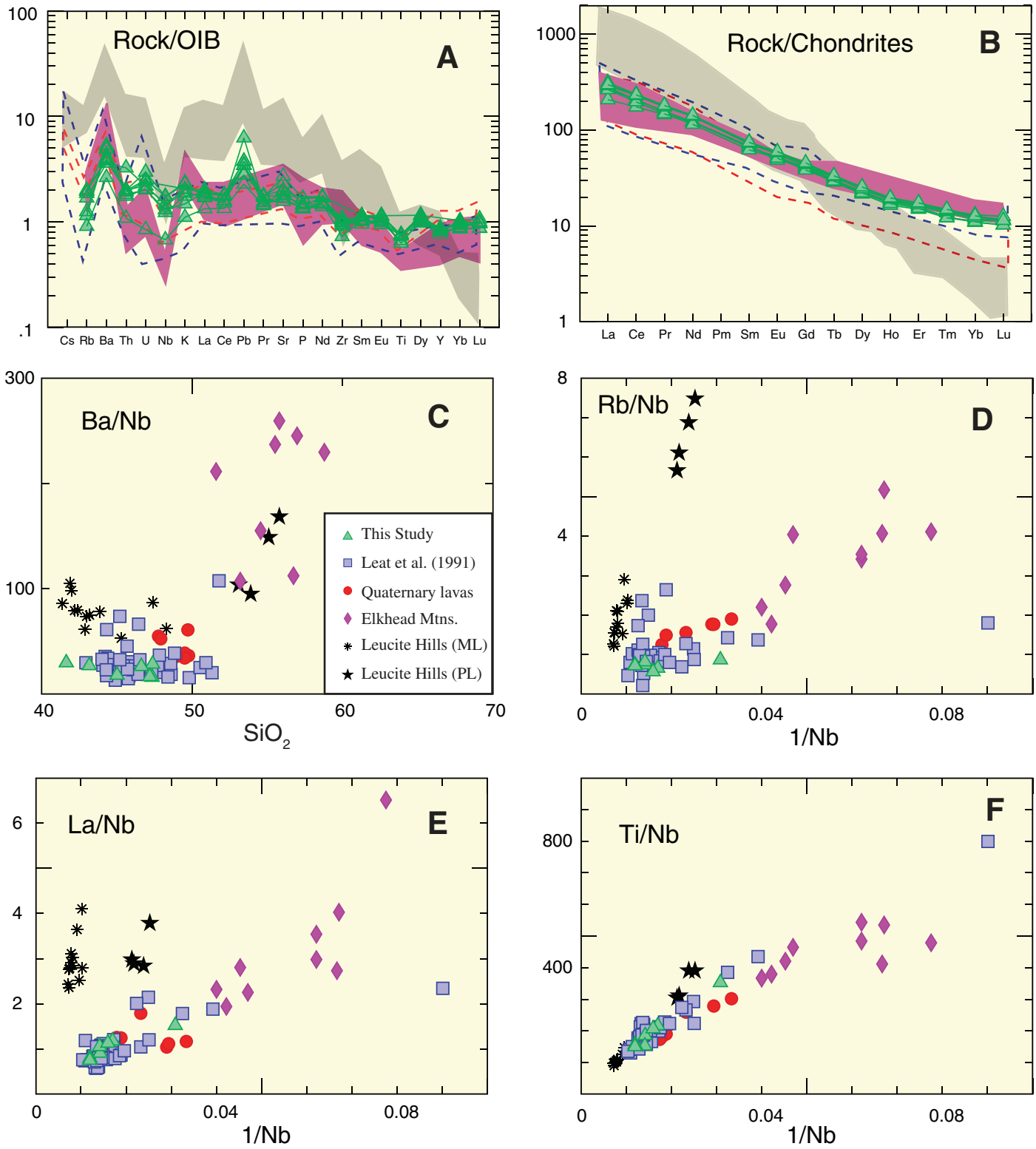

Figure 10. Trace element and rare earth element (REE) plots of Yampa lavas compared to selected lavas from northern Colorado and southwestern Wyoming. (A) Ocean island basalt (OIB) normalized trace element plots. (B) Chondrite normalized REE plots (Sun and McDonough, 1989) of Yampa lavas. Symbols: triangles—Yampa lavas (this study); blue dashed line—Yampa lavas (Leat et al., 1991); red dashed line—Quaternary basalts (Leat et al., 1989); pink shaded area—Elkhead Mountains (Thompson et al., 1990); gray shaded area—Leucite Hills lamproites (Mirnejad and Bell, 2006). (C–F) Selected trace element plots of Yampa lavas (sources of data as in Fig. 8). PL—phlogopite lamproite; ML—madupite lamproite.

TABLE 2. REPRESENTATIVE PHENOCRYST COMPOSITIONS FROM YAMPA LAVAS

Sample	10YV01A ol core	10YV01A ol rim	10YV05 ol core	10YV05 ol rim	10YV01A cpx core	10YV01A cpx rim	10YV02A cpx core	10YV02A cpx rim	10YV04A Ti-phl	10YV04A Ti-phl
SiO_2	39.39	38.96	40.71	39.28	50.96	47.37	48.58	41.78	36.84	36.29
TiO_2	0.02	0.01	0.03	0.04	0.30	2.48	1.53	4.04	7.72	7.80
Al_2O_3	0.02	0.04	0.03	0.01	2.37	6.77	6.32	10.96	17.64	17.34
Cr_2O_3	0.01	0.00	0.02	0.03	0.00	0.02	0.20	0.00	0.00	0.02
FeO	16.64	19.22	12.66	19.59	11.43	7.30	5.71	8.58	8.92	8.92
CoO	0.03	0.05	0.04	0.03	0.01	0.00	0.02	0.00	0.03	0.03
NiO	0.15	0.15	0.17	0.09	0.05	0.00	0.02	0.01	0.04	0.04
MnO	0.24	0.24	0.17	0.45	0.15	0.14	0.09	0.10	0.05	0.06
MgO	43.46	40.88	46.44	40.18	12.19	12.32	14.06	10.45	16.21	16.07
CaO	0.14	0.15	0.19	0.26	21.95	22.91	23.21	23.27	0.02	0.04
Na_2O	0.02	0.02	0.01	0.02	0.55	0.49	0.50	0.51	0.52	0.56
K_2O	0.00	0.00	0.00	0.02	0.00	0.00	0.02	0.00	9.82	9.63
P_2O_5	0.02	0.01	0.03	0.07	0.04	0.05	0.00	0.04	0.00	0.00
Total	100.12	99.73	100.50	100.07	99.99	99.87	100.25	99.74	97.83	96.81
Normalized cations per formula unit										
Si	0.996	1.002	1.008	1.011	1.914	1.765	1.782	1.569	5.420	5.397
Ti	0.000	0.000	0.000	0.001	0.008	0.070	0.042	0.114	0.854	0.872
Al	0.001	0.001	0.001	0.000	0.105	0.297	0.273	0.485	3.059	3.040
Cr	0.000	0.000	0.000	0.001	0.000	0.001	0.006	0.000	0.000	0.003
Fe_2+	0.352	0.414	0.262	0.422	0.359	0.227	0.175	0.269	1.097	1.110
Co	0.001	0.001	0.001	0.001	0.000	0.000	0.001	0.000	0.004	0.004
Ni	0.003	0.003	0.003	0.002	0.001	0.000	0.001	0.000	0.005	0.005
Mn	0.005	0.005	0.003	0.010	0.005	0.004	0.003	0.003	0.006	0.008
Mg	1.638	1.568	1.714	1.543	0.683	0.684	0.769	0.585	3.555	3.563
Ca	0.004	0.004	0.005	0.007	0.883	0.915	0.912	0.936	0.004	0.007
Na	0.001	0.002	0.000	0.001	0.040	0.035	0.036	0.037	0.148	0.161
K	0.000	0.000	0.000	0.001	0.000	0.000	0.001	0.000	1.842	1.828
P	0.000	0.000	0.001	0.002	0.001	0.002	0.000	0.001		

Note: Number of ions on the basis of (Si + Ti + Al + Fe + Cr + Co + Ni +Mn + Mg + Ca) = 3 (olivine); = 4 (clinopyroxene); = 12 (phlogopite); ol—olivine; cpx—clinopyroxene; Ti-phl—Ti-phlogopite.

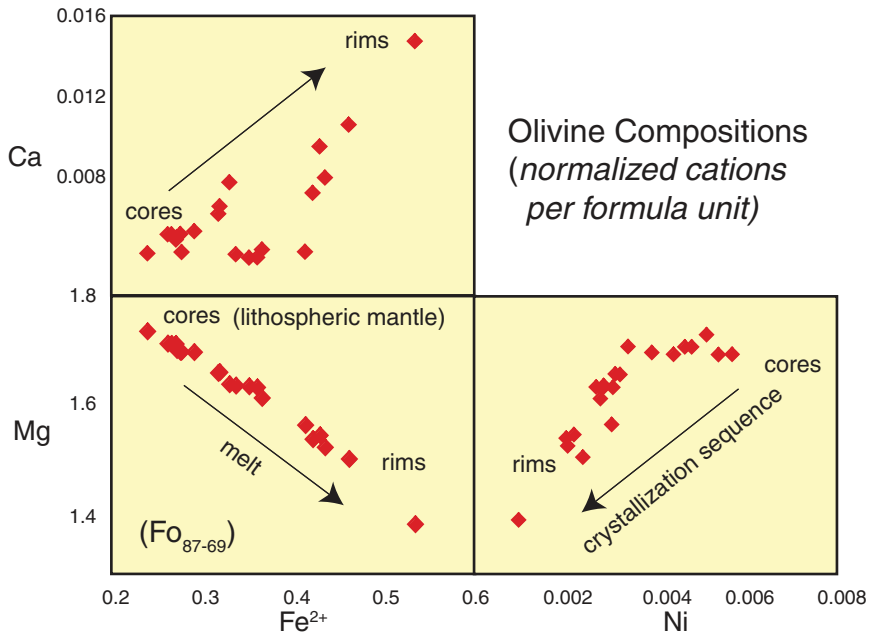

Figure 11. Plot of quantitative electron microprobe data measured in olivine core and rims from selected Yampa samples. Olivine stoichiometry normalized to 3 cations, with composition range of forsterite 87–69 ($Fo_{87–69}$). The Mg and Ni enrichment of the cores and Ca enrichment in rims are interpreted to record compositions of stable subcontinental lithospheric mantle and those precipitated from an evolving liquid-mineral interface during vertical ascension to the surface.

xenoliths have been reported that could be useful in defining the pressure and temperature conditions of the subcontinental lithospheric source region. However, core-to-rim mineral zoning and preservation of phenocrysts of Ti-phlogopite provide indirect evidence on the nature of the source region. Phlogopite is a mineral that likely contributes to the petrogenesis of alkaline magmas in continental settings (e.g., Lloyd and Bailey, 1975; Edgar, 1987; Foley, 1992; Pilet et al., 2011) and is stable in lherzolitic mantle to depths of 180–210 km at temperatures between 800 and 1200 °C (e.g., Konzett and Ulmer, 1999). A source for the Yampa lavas within the phlogopite stability field is consistent with partial melting of garnet peridotite (e.g., Beard and Johnson, 1993) and further supported by seismic tomography, which indicates a lithospheric thickness of ~150 km along the northeast margin of the Colorado Plateau (e.g., Dueker et al., 2001; Zurek and Dueker, 2005).

The core-to-rim zoning of both olivine and clinopyroxene phenocrysts in the Yampa lavas records distinct stages of mineral crystallization, one within the subcontinental lithospheric mantle and a second in contact with a compositionally varying melt during late Miocene extension. Relative to the phenocryst rims, the

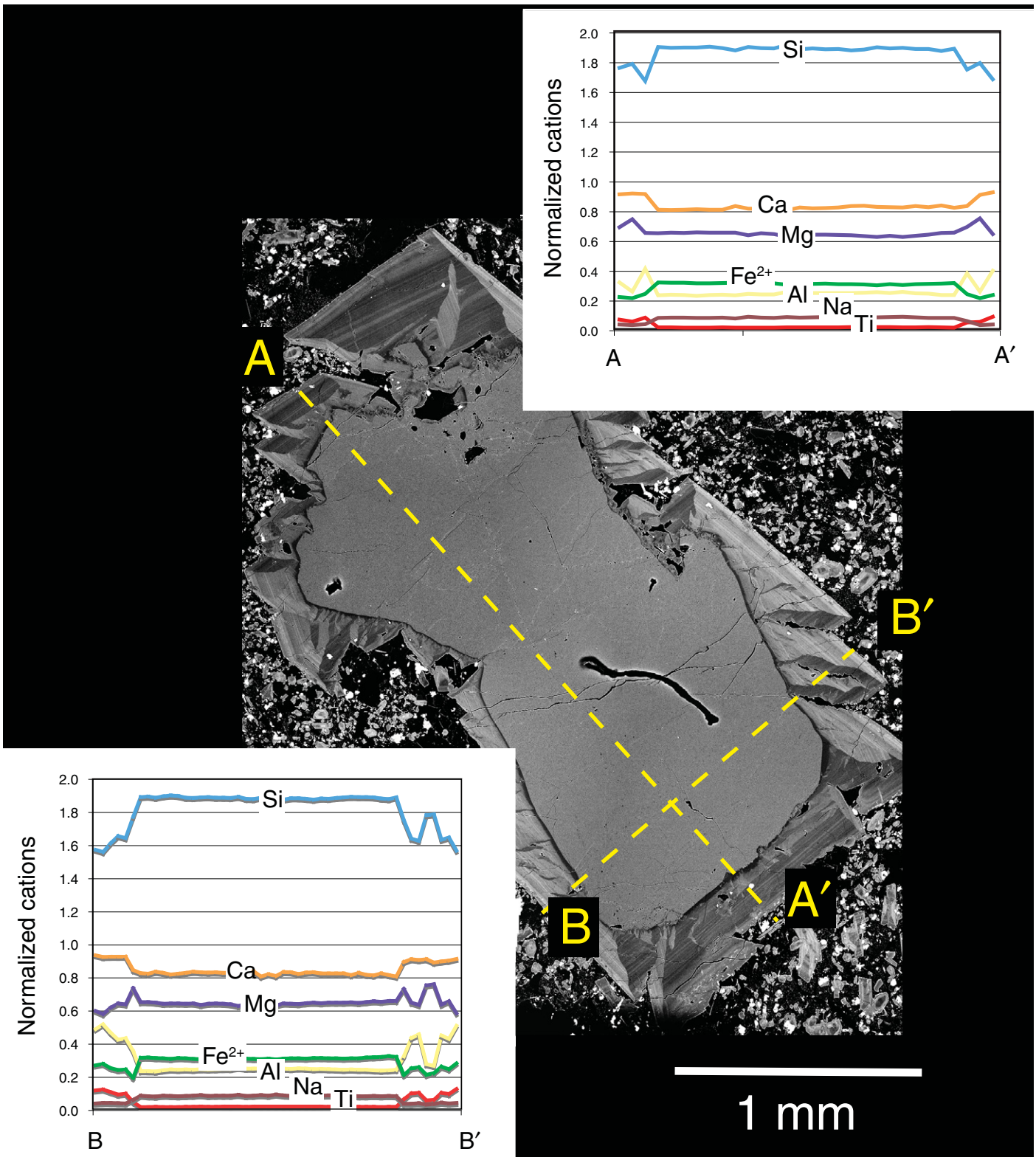

Figure 12. Backscattered electron image of large clinopyroxene with normalized cation (n = 4) concentrations plotted along two perpendicular traverses across the grain. Note the constant composition of the clinopyroxene core and the sharp transition to a compositionally distinct and finely banded rim. Preservation of this compositional transition, with rims enriched in Ca, Al, and Ti and depleted in Si, Mg, Fe, and Na relative to the core reflects a two-stage history of mineral growth. The clinopyroxene core compositions reflect those of the stable subcontinental lithospheric mantle and the rim compositions reflect mineral overgrowths tracking changes in melt compositions as the lithospheric mantle was partially melted during heating between 4.5 and 6 Ma.

TABLE 3. Rb-Sr, Sm-Nd, AND U-Th-Pb DATA FOR YAMPA BASALTS

Sample	Mass (mg)	U (ppm)	Th (ppm)	Pb (ppm)	$^{206}Pb/^{204}Pb^*$	$^{207}Pb/^{204}Pb^*$	$^{208}Pb/^{204}Pb^*$	$^{238}U/^{204}Pb^*$	$^{232}Th/^{204}Pb^*$	$^{206}Pb/^{204}Pb^\dagger$ (initial)	$^{207}Pb/^{204}Pb^\dagger$ (initial)	$^{208}Pb/^{204}Pb^\dagger$ (initial)
10YV-O1A	191	2.48	6.78	7.08	17.961	15.484	37.498	21.84	61.61	17.944	15.483	37.483
10YV-O2	157	2.25	7.02	22.7	17.970	15.513	37.612	6.19	19.95	17.994	15.513	37.607
10YV-O4A	204	2.3	7.48	7.42	17.893	15.487	37.431	19.27	64.67	17.878	15.486	37.415
10YV-O4B	162	2.87	7.15	7.19	17.883	15.477	37.392	24.76	63.75	17.864	15.476	37.376
10YV-O5	179	2.25	7.76	8.31	17.998	15.483	37.540	16.84	60.06	17.985	15.482	37.525
10YV-O6	183	0.818	4.06	4.77	17.516	15.439	37.309	10.55	54.10	17.508	15.439	37.296
10YV-O7	166	1.75	6.18	6.51	17.966	15.499	37.545	16.73	61.06	17.953	15.498	37.530

Sample	Mass (mg)	Rb§ (ppm)	Sr§ (ppm)	Sm§ (ppm)	Nd§ (ppm)	$^{87}Rb/^{86}Sr^{**}$	$^{87}Sr/^{86}Sr^{**}$	$^{147}Sm/^{144}Nd^{**}$	$^{143}Nd/^{144}Nd^{**}$	$^{87}Sr/^{86}Sr^{\dagger\dagger}$ (initial)	εNd (t)	T_{DM} model ages (Ma)
10YV-O1A	191	53.8	1209	10.72	62.36	0.1288	0.704238	0.10353	0.512400	0.70423	–4.6	895
10YV-O2	157	62.5	1929	10.63	62.36	0.0937	0.70509	0.10270	0.512452	0.70508	–3.6	815
10YV-O4A	204	105.8	764	9.27	51.74	0.4004	0.704144	0.10790	0.512542	0.70412	–1.8	730
10YV-O4B	162	81.2	1041	9.17	51.24	0.2258	0.704088	0.10780	0.512561	0.70407	–1.5	705
10YV-O5	179	84.0	1522	9.91	58.29	0.1598	0.705124	0.10237	0.512553	0.70511	–1.6	680
10YV-O6	183	37.9	1135	10.00	55.25	0.0966	0.705173	0.10898	0.512327	0.70517	–6.0	1040
10YV-O7	166	67.3	940	9.02	48.90	0.2071	0.704174	0.11114	0.512547	0.70416	–1.7	745

Note: T_{DM} is depleted mantle model age.

*Corrected for mass fractionation (0.08% per amu) and blank Pb (~110 pg total Pb) using the programming of Ludwig (1992).

†Initial ratios, calculated by subtracting the amount of ^{206}Pb, ^{207}Pb, and ^{208}Pb accumulated from the decay of U and Th in each sample since the formation of the rock, taken to be the best known radiometric age.

§Concentration uncertainties for Rb and Sr are ~1.0% and ~0.5%, respectively. Concentration uncertainties for Sm and Nd are ~0.5% and ~0.1%, respectively.

**Isotopic ratios corrected for blank and mass fractionation, $^{87}Sr/^{86}Sr$ data are normalized to $^{86}Sr/^{88}Sr = 0.1194$ and monitored for instrumental bias using NBS SRM 987 standard (see text). The mean $^{87}Sr/^{86}Sr$ value for 30 analyses of the Sr standard was 0.710265 ± 10. Uncertainties correspond to the last significant figures at the 95% confidence level. Isotopic ratios corrected for blank and mass fractionation, $^{143}Nd/^{144}Nd$ data are normalized to $^{146}Nd/^{144}Nd = 0.7219$ and monitored for instrumental bias using the La Jolla Nd standard. The mean value of $^{143}Nd/^{144}Nd$ for 30 analyses of the La Jolla Nd standard was 0.511865 ±10. Uncertainties correspond to the last significant figures at the 95% confidence level.

††Initial $^{87}Sr/^{86}Sr$ ratios were calculated using known age: $\lambda = 1.42 \times 10^{-11}yr^{-1}$; present-day ($^{87}Sr/^{86}Sr)UR = 0.7045$, and ($^{87}Rb/^{86}Sr)UR = 0.0824$ (UR is uniform reservoir). Initial $^{143}Nd/^{144}Nd$ ratios and εNd are calculated using known age (t): $\lambda = 6.54 \times 10^{-12}yr^{-1}$; present-day ($^{143}Nd/^{144}Nd)CHUR = 0.512636$, and ($^{147}Sm/^{144}Nd)CHUR = 0.1967$ (CHUR is chondritic uniform reservoir).

uniform compositions in phenocryst cores of clinopyroxene (enriched in Na and Si) and olivine (enriched in Mg and Ni) support residence at greater pressure. Olivine phenocryst rims have less Mg and Ni (Fig. 11), and clinopyroxene phenocryst rims have less Na and Al and are significantly enriched in Ti (Fig. 12). The larger phenocrysts, with a small jadeite component, are clearly melting, as evidenced by the numerous melt pools in most large grains. The fine-scale compositional bands developed along the clinopyroxene rims reflects changes in the melt compositions with which they were in contact over time scales of mineral growth. The compositionally uniform phenocryst cores, together with regular compositional trends preserved in the fine bands surrounding most phenocrysts, represent the overall transition from the subcontinental lithospheric mantle to the continental crust prior to eruption.

Late Cenozoic Migration of Alkaline Volcanism in Northwest Colorado

The nepheline-normative alkaline lavas of the Yampa volcanic field are volumetrically minor, but they are geodynamically important because they have geochemical signatures characteristic of incipient continental rifts (Carmichael et al., 1996). The alkaline and mafic lavas of the Yampa volcanic field were erupted between 4.5 and 6 Ma, and even at the scale of the field, the resolution of the $^{40}Ar/^{39}Ar$ data is sufficient to identify an overall southwestward temporal migration of magmatism (Fig. 3). At a slightly larger regional scale, and assuming that published K-Ar data are reliable, the Yampa volcanic field is one example of several occurrences of Pliocene to Quaternary alkalic volcanism that is progressively younger in the direction of the Colorado Plateau (Fig. 16). We interpret these rocks to represent partial melts from the subcontinental lithospheric mantle generated at depths >75 km in the garnet peridotite field. Because they have little isotopic evidence of crustal assimilation, preservation of these rocks forcibly emplaced at the surface almost certainly requires that they were following deep lithospheric pathways toward the surface. The northwest-trending high-angle Neogene faults associated with the Yampa and other Pliocene to Quaternary volcanic fields in northwest Colorado provide compelling evidence that volcanism is following and intruding into migrating zones of maximum strain developing within the continental lithosphere. These Pliocene and younger volcanic rocks, combined with the geologic and geochemical observations presented here, reflect incipient rifting of an

otherwise stable subcontinental lithospheric mantle that is still active and consistent with global positioning measurements recording exceedingly slow yet measurable strain rates distributed broadly across this zone (Berglund et al., 2012). Quaternary rifting is limited to a zone subparallel to the northeastern margin of the Colorado Plateau extending at least as far north as the Leucite Hills (Fig. 16). The Quaternary volcanic rocks define the western limit of the Rio Grande rift, which diverges around the thick volcano-plutonic root of the southern Rocky Mountains volcanic field and tapers into thicker lithosphere at its north end.

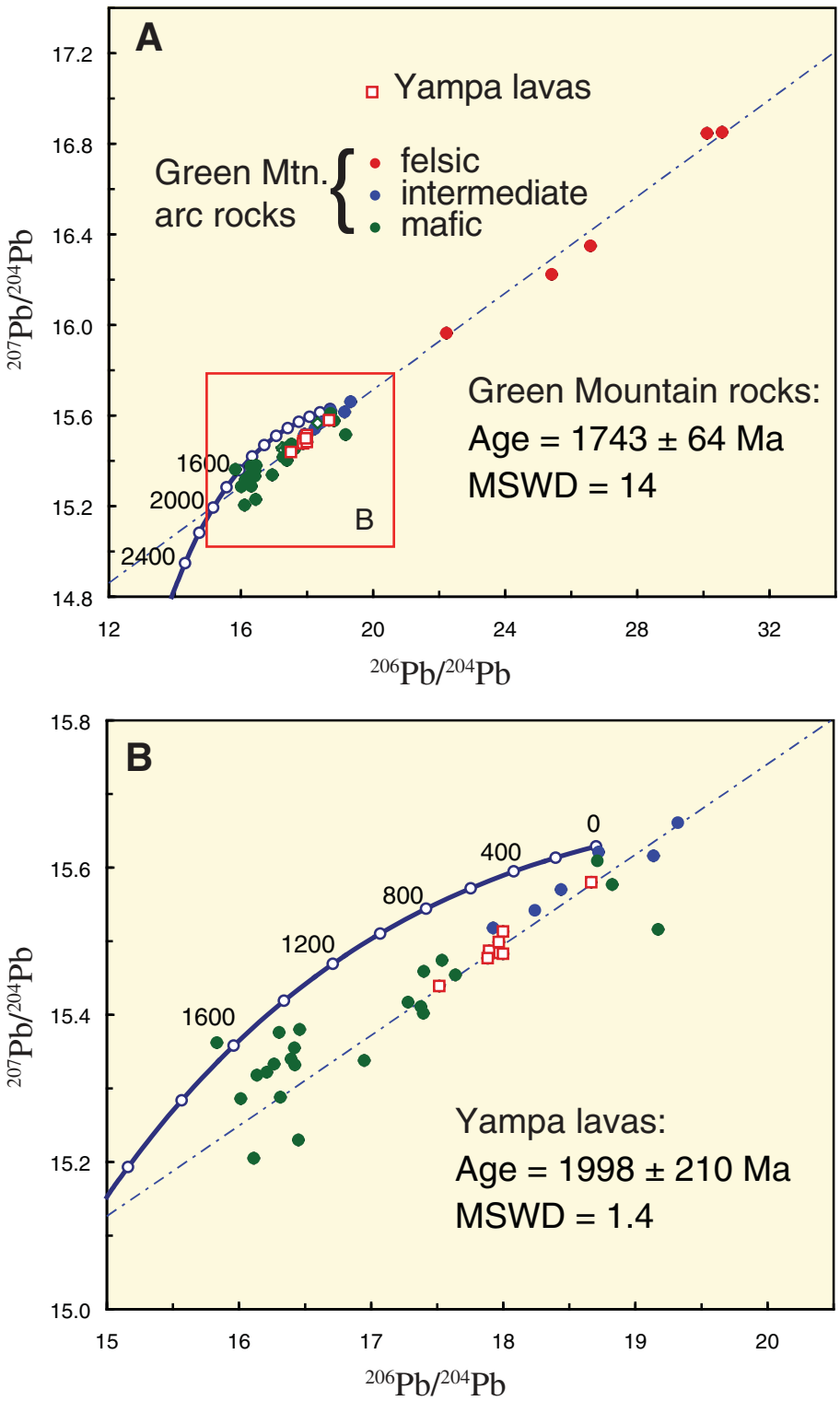

Figure 13. (A) $^{207}Pb/^{204}Pb$ versus $^{206}Pb/^{204}Pb$ isotope data from Yampa lavas plotted together with data from the Proterozoic Green Mountain arc in relation to the terrestrial Pb evolution model of Stacey and Kramers (1975). Typical errors are 0.1% for $^{206}Pb/^{204}Pb$ and 0.15% for $^{207}Pb/^{204}Pb$. (A) $^{207}Pb/^{204}Pb$ versus $^{206}Pb/^{204}Pb$ values of mafic, felsic, and intermediate composition Paleoproterozoic plutonic Green Mountain arc rocks from northwestern Colorado and southwestern Wyoming (Premo and Loucks, 2000). These data define a whole-rock Pb-Pb errorchron age of 1743 ± 64 Ma. Also plotted are the Pb isotopic compositions of the Yampa lavas. (B) Expanded part of diagram in A, which shows the similar Pb isotope compositions of the Yampa lavas to mafic rocks of the Proterozoic Green Mountain arc. The $^{207}Pb/^{204}Pb$ versus $^{206}Pb/^{204}Pb$ whole-rock isochron age of 1998 ± 210 Ma is poorly defined despite the low mean square of weighted deviates (MSWD) because of limited spread in the isotope ratios. All isochron plots and terrestrial Pb evolution diagrams were created using Isoplot (Ludwig, 2003).

Past and Present Magmatism within the Rio Grande Rift

Two regional episodes of late Cenozoic extension affected the Basin and Range province (e.g., Wernicke et al., 1987; Prodehl and Lipman, 1989; Dickinson, 2004), but only the younger episode seems to implicate the Rio Grande rift. An initial episode of Eocene to early Miocene extension is characterized by large calc-alkaline volcanic provinces and ignimbrite-forming calderas, including those of the southern Rocky Mountain volcanic field east of the Colorado Plateau (Lipman et al., 1971; Wernicke et al., 1987; Christiansen and Yeats, 1992; Dickinson, 2002; McIntosh and Chapin, 2004; Lipman and McIntosh, 2008). During that time, extension and igneous activity began and progressed from north to south in the northern Basin and Range province and began later and progressed from south to north in the southern Basin and Range province (Wernicke et al., 1987; Humphreys, 1995; Dickinson, 2002; Humphreys et al., 2003). Melting of mainly fertile Proterozoic (and minor Archean) lithosphere fluxed by devolatilization of subducted slab fragments may be responsible for volcanism of the western U.S. (e.g.,

Humphreys, 2009; Jones et al., 2011a). This volcanism generally coincides with Eocene extension and exhumation of metamorphic core complexes and Eocene to early Miocene calc-alkaline volcanic input into several large syntectonic basins in the northern Basin and Range province (Chamberlain et al., 2012).

A second episode of regional extension beginning ca. 20 Ma coincided with migration of triple junctions bounding the transform system (Fig. 1) that was subducting along the coast of western North America (e.g., Lipman et al., 1971; Ingersoll, 1982; Wernicke et al., 1987; Prodehl and Lipman, 1989; Jones et al., 1992; Atwater and Stock, 1998; Dickinson, 2002). As in other areas of the Basin and Range (e.g., Wernicke et al., 1987), this Miocene stage of extension in the Rio Grande rift corridor of Colorado and New Mexico is expressed by a transition from dominantly calc-alkaline magmatism to bimodal calc-alkaline and tholeiitic magmatism (e.g., Lipman, 1969; Lipman et al., 1971; Prodehl and Lipman, 1989; McMillan et al., 2000; Eaton, 2008; Chapin, 2012). In northwest Colorado the Elkhead Mountains, the Flat Tops Wilderness, and a few isolated eruptions apparently formed during this subsequent Miocene period of extension, and evidence of this extension was also recorded in the southern Colorado Plateau (e.g., Gonzales et al., 2010). Continued migration of the Rivera triple junction progressively affected the southern Basin and Range through the Pliocene and Quaternary, and is expressed by high-angle normal faults in northern Colorado and southern Wyoming, and coincided with an overall clockwise rotation in principal extension directions during the Pliocene from northeast-southwest to east-west (Prodehl and Lipman, 1989; Williams and Cole, 2007).

From 12 Ma to the present, bimodal volcanism within the Rio Grande rift corridor in New Mexico and southern Colorado reflects the ascent of asthenospheric mantle and its interaction with a thinning lithosphere (Lipman, 1969; Lipman and Mehnert, 1975). The first unequivocal asthenospheric magmas within the

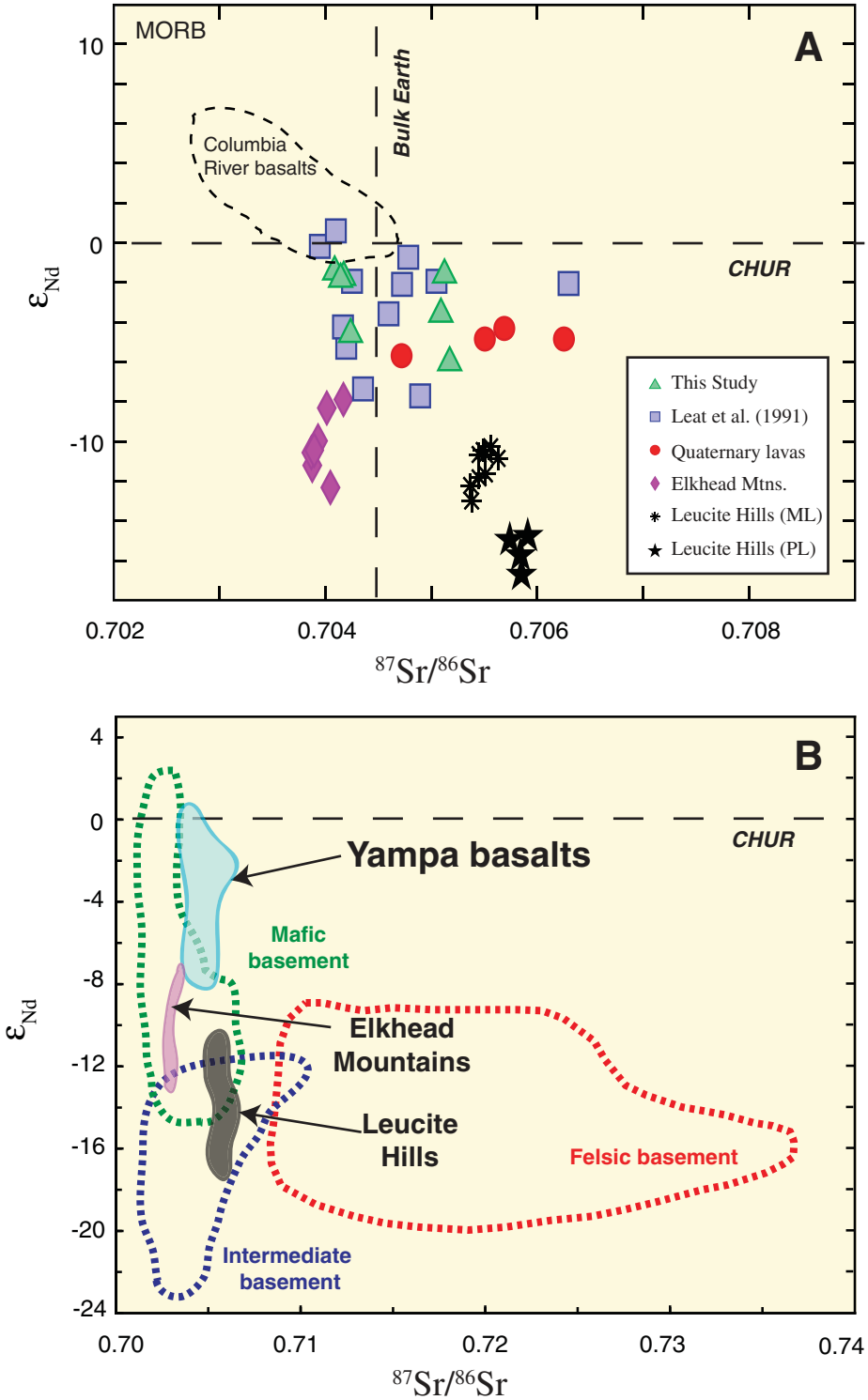

Figure 14. Sr and Nd isotope plots of Yampa lavas compared to locally occurring basement and igneous rocks. (A) ε_{Nd} versus $^{87}Sr/^{86}Sr$ plot of Yampa lavas (this study; Leat et al., 1991) plotted together with data from the Leucite Hills (Mirnejad, and Bell, 2006) and modern values of mafic, intermediate, and felsic basement samples of the Paleoproterozoic Green Mountain arc terrane (Premo and Loucks, 2000). Both the Nd and Sr isotopic results for the Yampa lavas plot close to source regions defined by mafic Proterozoic lithospheric basement underlying much of northern Colorado. MORB—mid-oceanic ridge basalt; PL—phlogopite lamproite; ML—madupite lamproite. (B) ε_{Nd} and Sr isotope plots of the Yampa lavas together with data from the Elkhead Mountains (Thompson et al., 1990), Leucite Hills (Mirnejad and Bell, 2006), and Quaternary basalts of northern Colorado (Leat et al., 1989). The Nd and Sr isotope data for all these rocks are consistent with Proterozoic or older lithospheric mantle sources. CHUR—chondritic uniform reservoir.

TABLE 4. ANALYTICAL RESULTS OF CO_2-LASER INCREMENTAL HEATING $^{40}Ar/^{39}Ar$ EXPERIMENTS

	Relative isotopic abundances (x 10^{-11}A)										Derived results									
Watts	^{40}Ar ±1σ		^{39}Ar ±1σ		^{38}Ar ±1σ		^{37}Ar ±1σ		^{36}Ar ±1σ		^{39}Ar Mol × 10^{-14}	^{39}Ar (% of total)	Ca/K ±1σ		$^{40}Ar^*/^{39}Ar$ ±1σ		$\%^{40}Ar^*$	Age (Ma) ±1σ	
10YV01A, whole rock, J = 0.000793 ± 0.000003; UTM coordinates 343949, 4440095																				
0.1	21.431	0.032	0.198	0.002	0.017	0.001	0.206	0.003	0.0689	0.0005	0.004	0.2	2.04	0.035	5.56	0.84	4.2	6.43	1.21
0.3	26.578	0.038	0.367	0.002	0.024	0.001	0.342	0.002	0.0841	0.0006	0.008	0.4	1.83	0.015	4.80	0.51	5.7	5.86	0.73
0.6	36.352	0.077	0.640	0.003	0.034	0.001	0.567	0.003	0.1132	0.0005	0.014	0.6	1.74	0.013	4.61	0.31	7.2	5.81	0.44
0.9	51.980	0.099	1.158	0.006	0.055	0.001	0.935	0.007	0.1541	0.0007	0.026	1.1	1.58	0.014	5.62	0.22	11.6	7.45	0.32
1.2	88.995	0.170	2.172	0.008	0.094	0.001	1.448	0.005	0.2597	0.0011	0.048	2.1	1.31	0.007	5.71	0.19	13.0	7.62	0.28
1.5	224.915	0.250	4.562	0.009	0.216	0.001	2.366	0.010	0.6791	0.0015	0.101	4.5	1.02	0.005	5.36	0.16	9.9	7.00	0.22
1.8	444.099	0.220	10.050	0.013	0.430	0.002	3.618	0.011	1.3174	0.0019	0.221	9.8	0.71	0.002	5.49	0.11	11.5	7.26	0.16
2.1	275.187	0.190	12.305	0.012	0.339	0.002	3.728	0.012	0.7326	0.0014	0.271	12.1	0.59	0.002	4.80	0.06	20.6	6.59	0.08
2.5	223.725	0.230	12.317	0.013	0.300	0.002	3.965	0.013	0.5636	0.0013	0.271	12.1	0.63	0.002	4.67	0.05	24.9	6.47	0.07
3.0	225.807	0.210	13.131	0.014	0.318	0.002	4.769	0.015	0.5659	0.0013	0.289	12.9	0.71	0.002	4.49	0.05	25.4	6.23	0.07
3.5	345.479	0.190	21.101	0.017	0.471	0.002	12.884	0.024	0.8511	0.0017	0.465	20.7	1.20	0.002	4.51	0.04	26.8	6.26	0.06
4.0	150.350	0.150	10.492	0.013	0.209	0.002	13.278	0.027	0.3567	0.0020	0.231	10.3	2.48	0.006	4.39	0.06	29.9	6.13	0.09
4.5	374.285	0.350	11.685	0.011	0.378	0.001	31.612	0.070	1.0870	0.0031	0.257	11.4	5.30	0.013	4.77	0.11	14.0	6.41	0.16
5.0	46.734	0.048	1.912	0.005	0.054	0.001	5.125	0.017	0.1287	0.0012	0.042	1.9	5.25	0.022	4.78	0.20	18.7	6.53	0.28
10YV01B, whole rock, J = 0.000793 ± 0.000003; UTM coordinates 343949, 4440095																				
0.5	18.246	0.039	0.740	0.003	0.025	0.001	0.730	0.005	0.0533	0.0005	0.016	0.5	1.93	0.016	3.45	0.22	13.1	4.61	0.31
0.8	46.952	0.047	1.127	0.003	0.047	0.001	0.831	0.005	0.1380	0.0007	0.025	0.8	1.45	0.010	5.54	0.21	12.4	7.37	0.30
1.0	959.868	0.400	3.706	0.007	0.671	0.003	1.995	0.009	3.1178	0.0031	0.082	2.6	1.05	0.005	10.45	0.66	3.0	11.23	0.94
1.3	1162.422	0.550	5.755	0.009	0.818	0.002	2.485	0.009	3.7426	0.0036	0.127	4.0	0.85	0.003	9.85	0.51	3.9	11.21	0.73
1.5	672.742	0.310	6.896	0.010	0.508	0.002	2.224	0.008	2.1206	0.0023	0.152	4.8	0.63	0.002	6.72	0.25	5.9	8.24	0.35
1.8	826.881	0.330	8.989	0.011	0.640	0.002	3.026	0.009	2.5945	0.0029	0.198	6.2	0.66	0.002	6.73	0.23	6.4	8.34	0.33
2.1	917.875	0.310	10.674	0.011	0.710	0.002	3.874	0.014	2.8731	0.0031	0.235	7.4	0.71	0.003	6.48	0.21	6.6	8.08	0.31
2.5	724.746	0.280	13.605	0.019	0.611	0.002	5.125	0.013	2.2035	0.0024	0.300	9.4	0.74	0.002	5.44	0.13	9.3	7.06	0.19
3.0	394.050	0.320	13.756	0.014	0.398	0.002	6.108	0.015	1.1081	0.0018	0.303	9.5	0.87	0.002	4.88	0.08	16.2	6.62	0.11
3.5	1633.042	0.550	27.227	0.035	1.330	0.003	20.483	0.034	4.9917	0.0039	0.600	18.8	1.47	0.003	5.87	0.14	8.8	7.57	0.20
4.0	2069.428	0.660	37.448	0.051	1.725	0.004	62.822	0.083	6.3342	0.0120	0.825	25.9	3.29	0.006	5.42	0.16	8.9	7.00	0.22
4.5	547.595	0.270	11.915	0.012	0.483	0.002	39.479	0.044	1.6527	0.0023	0.262	8.2	6.49	0.010	5.25	0.12	10.5	6.90	0.17
5.0	111.592	0.102	2.631	0.006	0.101	0.001	11.310	0.034	0.3325	0.0022	0.058	1.8	8.42	0.032	5.43	0.27	11.9	7.21	0.39
10YV02A, whole rock, J = 0.000793 +/- 0.000003; UTM coordinates 343827, 4440472																				
0.5	158.526	0.450	1.888	0.005	0.131	0.001	1.353	0.007	0.5132	0.0014	0.042	1.2	1.41	0.008	3.71	0.38	7.0	8.76	0.48
0.8	286.678	0.620	3.961	0.005	0.243	0.002	1.478	0.007	0.9255	0.0018	0.087	2.5	0.73	0.004	3.37	0.27	6.5	6.92	0.34
1.0	333.226	1.000	6.006	0.007	0.303	0.002	2.213	0.006	1.0583	0.0020	0.132	3.8	0.72	0.002	3.45	0.23	5.2	4.15	0.34
1.3	350.756	1.100	7.219	0.016	0.320	0.002	2.601	0.010	1.1138	0.0021	0.159	4.6	0.71	0.003	3.03	0.21	5.3	3.65	0.30
1.5	364.663	1.100	8.189	0.008	0.339	0.002	2.657	0.011	1.1463	0.0023	0.180	5.2	0.64	0.003	3.19	0.19	6.2	3.95	0.27
1.8	380.901	1.200	9.777	0.011	0.356	0.002	3.219	0.010	1.1596	0.0023	0.215	6.2	0.65	0.002	3.94	0.17	9.2	5.11	0.24
2.1	330.810	1.000	10.156	0.011	0.323	0.002	4.170	0.021	0.9902	0.0019	0.224	6.4	0.80	0.004	3.80	0.14	10.7	5.00	0.19
2.5	341.592	1.100	10.540	0.011	0.329	0.002	4.842	0.015	1.0072	0.0019	0.232	6.7	0.90	0.003	4.21	0.14	12.1	5.60	0.20
3.0	406.340	0.540	14.083	0.021	0.392	0.002	5.015	0.011	1.1119	0.0053	0.310	8.9	0.70	0.002	5.55	0.13	18.4	7.58	0.19
3.5	385.367	0.620	26.572	0.063	0.494	0.002	7.173	0.022	0.8626	0.0044	0.585	16.8	0.53	0.002	4.93	0.06	33.3	6.90	0.09
4.0	280.779	0.191	39.044	0.051	0.566	0.002	37.860	0.104	0.3757	0.0011	0.860	24.7	1.90	0.006	4.43	0.01	61.2	6.29	0.02
4.5	129.638	0.131	17.469	0.020	0.266	0.002	60.280	0.149	0.1939	0.0009	0.385	11.0	6.76	0.019	4.43	0.02	59.2	6.29	0.03
5.0	25.246	0.049	3.455	0.007	0.052	0.001	11.338	0.030	0.0376	0.0007	0.076	2.2	6.43	0.022	4.37	0.06	59.3	6.20	0.09

(*Continued*)

TABLE 4. ANALYTICAL RESULTS OF CO_2-LASER INCREMENTAL HEATING $^{40}Ar/^{39}Ar$ EXPERIMENTS (*Continued*)

	Relative isotopic abundances (x 10^{-11}A)										Derived results									
Watts	^{40}Ar	±1σ	^{39}Ar	±1σ	^{38}Ar	±1σ	^{37}Ar	±1σ	^{36}Ar	±1σ	^{39}Ar Mol × 10^{-14}	^{39}Ar (% of total)	Ca/K	±1σ	$^{40}Ar^*/^{39}Ar$	±1σ	$\%^{40}Ar^*$	Age (Ma)	±1σ
10YV02B, whole rock, J = 0.000793 ± 0.000003; UTM coordinates 343827, 4440472																				
0.5	416.985	0.250	5.407	0.009	0.337	0.003	5.076	0.020	1.3456	0.0020	0.119	3.6	1.84	0.008	2.90	0.22	3.8	4.14	0.31
0.8	504.556	0.870	7.677	0.017	0.410	0.005	3.689	0.011	1.6169	0.0026	0.170	5.2	0.94	0.004	2.88	0.22	4.4	4.12	0.31
1.2	584.280	1.100	10.855	0.010	0.495	0.004	4.986	0.013	1.8657	0.0030	0.240	7.3	0.90	0.003	2.55	0.18	4.7	3.65	0.26
1.3	501.885	1.300	10.408	0.017	0.422	0.003	4.098	0.017	1.5463	0.0024	0.230	7.0	0.77	0.003	3.90	0.18	8.1	5.57	0.26
1.5	339.820	0.950	9.556	0.018	0.313	0.002	5.062	0.016	1.0226	0.0020	0.211	6.4	1.04	0.004	3.66	0.14	10.3	5.23	0.20
1.8	288.339	1.100	9.002	0.016	0.280	0.002	6.582	0.015	0.8573	0.0025	0.199	6.1	1.43	0.004	3.66	0.17	11.4	5.23	0.24
2.1	503.219	1.200	10.050	0.009	0.423	0.003	5.430	0.019	1.5334	0.0033	0.222	6.8	1.06	0.004	4.56	0.19	9.1	6.52	0.27
2.5	711.356	0.550	30.218	0.059	0.738	0.003	7.830	0.023	1.8842	0.0062	0.667	20.3	0.51	0.002	4.95	0.08	21.0	7.06	0.11
3.0	267.340	0.240	31.413	0.045	0.476	0.003	14.972	0.037	0.4362	0.0013	0.694	21.1	0.93	0.003	4.41	0.02	51.7	6.29	0.03
3.5	97.124	0.088	12.700	0.019	0.186	0.002	23.848	0.054	0.1479	0.0008	0.281	8.5	3.68	0.010	4.33	0.02	56.6	6.19	0.03
4.0	50.331	0.053	6.220	0.016	0.095	0.001	19.143	0.049	0.0848	0.0008	0.137	4.2	6.03	0.022	4.28	0.04	52.8	6.12	0.06
4.5	19.269	0.041	2.300	0.009	0.032	0.001	8.655	0.063	0.0340	0.0006	0.051	1.5	7.38	0.062	4.29	0.08	51.1	6.13	0.11
5.0	13.776	0.030	1.493	0.004	0.023	0.001	7.020	0.028	0.0265	0.0005	0.033	1.0	9.22	0.044	4.32	0.11	46.7	6.17	0.16
5.5	6.875	0.017	0.720	0.003	0.013	0.001	3.233	0.014	0.0152	0.0005	0.016	0.5	8.80	0.057	3.63	0.22	37.9	5.18	0.31
6.0	5.379	0.018	0.582	0.002	0.009	0.001	2.490	0.022	0.0119	0.0005	0.013	0.4	8.39	0.081	3.52	0.26	38.0	5.03	0.37
10YV04B, whole rock, J = 0.000793 ± 0.000003; UTM coordinates 342464, 4440505																				
0.5	135.800	0.180	3.195	0.006	0.154	0.001	2.408	0.010	0.3996	0.0010	0.070	0.8	1.48	0.007	5.61	0.14	13.2	8.01	0.21
0.8	183.849	0.560	13.009	0.020	0.283	0.001	6.553	0.019	0.4711	0.0012	0.286	3.4	0.99	0.003	3.47	0.06	24.6	4.96	0.08
1.2	371.338	0.610	56.288	0.082	0.842	0.003	19.501	0.035	0.5810	0.0015	1.240	14.7	0.68	0.002	3.58	0.02	54.2	5.11	0.02
1.5	433.431	0.360	75.966	0.070	1.099	0.003	23.756	0.033	0.5572	0.0013	1.673	19.8	0.61	0.001	3.56	0.01	62.5	5.09	0.02
1.8	389.173	0.210	69.676	0.084	0.980	0.003	18.023	0.024	0.4720	0.0013	1.534	18.2	0.51	0.001	3.61	0.01	64.5	5.15	0.01
2.1	216.073	0.210	43.414	0.066	0.597	0.002	9.041	0.023	0.2122	0.0009	0.956	11.3	0.41	0.001	3.55	0.01	71.3	5.07	0.02
2.5	157.441	0.150	32.308	0.049	0.438	0.003	6.773	0.017	0.1464	0.0011	0.711	8.4	0.41	0.001	3.55	0.01	72.9	5.07	0.02
3.0	221.271	0.210	42.767	0.064	0.594	0.004	13.192	0.030	0.2393	0.0010	0.942	11.2	0.60	0.002	3.55	0.01	68.5	5.07	0.02
3.5	204.232	0.150	34.106	0.052	0.503	0.002	23.213	0.043	0.2880	0.0009	0.751	8.9	1.33	0.003	3.55	0.01	59.3	5.07	0.02
4.0	31.745	0.038	4.679	0.008	0.073	0.001	2.987	0.011	0.0543	0.0006	0.103	1.2	1.25	0.005	3.41	0.04	50.2	4.87	0.06
4.5	18.329	0.029	2.694	0.005	0.041	0.001	1.819	0.014	0.0292	0.0005	0.059	0.7	1.32	0.011	3.66	0.06	53.7	5.22	0.09
5.0	23.458	0.040	3.337	0.006	0.052	0.001	3.316	0.012	0.0411	0.0005	0.074	0.9	1.95	0.008	3.48	0.05	49.4	4.97	0.07
5.5	10.965	0.019	1.557	0.004	0.026	0.001	1.564	0.009	0.0205	0.0005	0.034	0.4	1.97	0.013	3.24	0.09	45.9	4.62	0.13
10YV05A, whole rock, J = 0.000776 ± 0.000003; UTM coordinates 338937, 4443175																				
0.5	156.933	0.190	4.309	0.010	0.161	0.001	2.841	0.015	0.4564	0.0023	0.095	2.6	1.29	0.008	5.18	0.18	14.2	7.23	0.26
0.8	172.279	0.400	3.908	0.013	0.166	0.002	3.573	0.009	0.5215	0.0015	0.086	2.4	1.79	0.008	4.73	0.18	10.7	6.61	0.26
1.2	230.194	0.580	4.752	0.014	0.209	0.002	4.847	0.011	0.6991	0.0018	0.105	2.9	2.00	0.008	5.05	0.20	10.4	7.06	0.28
1.5	237.968	0.520	7.206	0.017	0.234	0.002	6.616	0.028	0.7025	0.0018	0.159	4.3	1.80	0.009	4.29	0.13	13.0	6.00	0.18
1.8	266.497	0.580	10.083	0.023	0.281	0.002	8.609	0.028	0.7597	0.0017	0.222	6.1	1.67	0.007	4.24	0.10	16.0	5.92	0.13
2.1	286.944	0.510	11.507	0.019	0.306	0.002	8.738	0.019	0.8162	0.0019	0.253	6.9	1.49	0.004	4.04	0.09	16.2	5.65	0.12
2.5	379.120	0.500	16.040	0.027	0.412	0.002	10.376	0.021	1.0673	0.0021	0.353	9.6	1.27	0.003	4.03	0.07	17.0	5.63	0.10
3.0	519.329	0.380	30.601	0.065	0.646	0.003	17.406	0.054	1.3598	0.0029	0.674	18.4	1.11	0.004	3.89	0.05	22.9	5.43	0.06
3.5	278.038	0.270	34.239	0.070	0.538	0.003	16.966	0.033	0.5436	0.0015	0.754	20.6	0.97	0.003	3.47	0.02	42.7	4.85	0.03
4.0	137.143	0.180	20.195	0.025	0.307	0.002	13.745	0.049	0.2400	0.0010	0.445	12.1	1.33	0.005	3.34	0.02	49.1	4.66	0.03
4.5	83.260	0.110	10.368	0.019	0.170	0.001	14.233	0.025	0.1626	0.0009	0.228	6.2	2.69	0.007	3.51	0.03	43.7	4.91	0.04
5.0	66.082	0.098	5.984	0.014	0.110	0.001	16.447	0.028	0.1527	0.0010	0.132	3.6	5.39	0.016	3.74	0.06	33.8	5.22	0.08
5.5	60.284	0.097	4.488	0.009	0.087	0.001	14.012	0.046	0.1459	0.0009	0.099	2.7	6.12	0.024	4.09	0.07	30.4	5.71	0.10
6.0	40.652	0.076	2.561	0.007	0.057	0.001	8.813	0.018	0.1043	0.0009	0.056	1.5	6.74	0.024	4.13	0.11	26.0	5.77	0.15

(*Continued*)

TABLE 4. ANALYTICAL RESULTS OF CO_2-LASER INCREMENTAL HEATING $^{40}Ar/^{39}Ar$ EXPERIMENTS (*Continued*)

	Relative isotopic abundances (x 10^{-11}A)										Derived results									
Watts	^{40}Ar	±1σ	^{39}Ar	±1σ	^{38}Ar	±1σ	^{37}Ar	±1σ	^{36}Ar	±1σ	^{39}Ar Mol × 10^{-14}	^{39}Ar (% of total)	Ca/K	±1σ	$^{40}Ar^*/^{39}Ar$	±1σ	$\%^{40}Ar^*$	Age (Ma)	±1σ
10YV05B, whole rock, J = 0.000776 ± 0.000003; UTM coordinates 338937, 4443175																				
0.5	591.092	0.360	2.971	0.013	0.407	0.004	4.169	0.014	1.9018	0.0036	0.066	1.5	2.75	0.015	7.97	0.60	4.0	11.11	0.84
0.8	742.211	1.100	5.151	0.014	0.537	0.006	6.057	0.017	2.3500	0.0039	0.114	2.6	2.30	0.009	7.98	0.46	5.5	11.14	0.64
1.3	575.451	0.350	11.831	0.026	0.490	0.002	8.680	0.034	1.7495	0.0030	0.261	6.1	1.44	0.006	4.55	0.14	9.4	6.36	0.19
1.5	514.722	0.360	16.796	0.033	0.489	0.004	7.827	0.019	1.5069	0.0033	0.371	8.6	0.91	0.003	3.90	0.09	12.7	5.45	0.13
1.8	693.805	0.550	23.022	0.056	0.680	0.004	9.364	0.028	2.0224	0.0027	0.509	11.8	0.80	0.003	3.94	0.08	13.1	5.51	0.11
2.1	886.680	0.680	54.345	0.100	1.137	0.006	20.403	0.045	2.3050	0.0035	1.200	27.8	0.74	0.002	3.68	0.04	22.6	5.15	0.06
2.5	390.098	0.260	49.391	0.100	0.714	0.010	18.581	0.045	0.7631	0.0018	1.091	25.3	0.74	0.002	3.32	0.02	42.0	4.64	0.03
3.5	273.555	0.240	18.325	0.042	0.343	0.004	24.956	0.055	0.5544	0.0018	0.405	9.4	2.67	0.009	6.01	0.04	40.2	8.40	0.06
4.5	188.411	0.200	6.621	0.014	0.143	0.003	6.078	0.023	0.2600	0.0014	0.146	3.4	1.80	0.008	16.82	0.09	59.1	23.38	0.12
5.5	203.172	0.180	7.053	0.019	0.148	0.002	8.396	0.018	0.2979	0.0013	0.156	3.6	2.33	0.008	16.31	0.08	56.6	22.67	0.12
10YV06, whole rock, J = 0.000776 ± 0.000003; UTM coordinates 335977, 4449048																				
0.5	328.296	0.380	5.132	0.008	0.222	0.001	5.679	0.015	0.7988	0.0017	0.113	4.2	2.17	0.007	18.08	0.18	28.2	25.12	0.24
0.8	234.661	0.350	11.116	0.013	0.157	0.001	10.053	0.025	0.1178	0.0009	0.245	9.0	1.77	0.005	18.06	0.05	85.5	25.10	0.07
1.2	159.972	0.290	8.120	0.012	0.113	0.001	7.585	0.018	0.0677	0.0007	0.179	6.6	1.83	0.005	17.32	0.05	87.9	24.08	0.08
1.5	136.648	0.170	6.544	0.010	0.099	0.001	7.126	0.022	0.0884	0.0007	0.144	5.3	2.13	0.007	16.99	0.05	81.3	23.62	0.07
1.8	132.676	0.120	6.992	0.014	0.099	0.001	8.749	0.031	0.0518	0.0006	0.154	5.7	2.45	0.010	16.91	0.05	89.0	23.50	0.07
2.1	100.321	0.097	5.498	0.008	0.080	0.001	7.505	0.020	0.0345	0.0006	0.121	4.5	2.68	0.008	16.52	0.05	90.5	22.97	0.06
2.5	74.954	0.078	4.062	0.007	0.064	0.001	6.929	0.031	0.0382	0.0005	0.089	3.3	3.34	0.016	15.83	0.05	85.7	22.02	0.07
3.0	213.717	0.150	10.615	0.015	0.175	0.002	18.627	0.063	0.1616	0.0008	0.234	8.6	3.44	0.013	15.80	0.04	78.4	21.97	0.06
3.5	202.745	0.160	10.396	0.012	0.170	0.001	23.841	0.039	0.1426	0.0008	0.229	8.4	4.50	0.009	15.66	0.04	80.2	21.78	0.05
4.0	159.699	0.140	8.366	0.014	0.139	0.001	21.027	0.031	0.1051	0.0007	0.184	6.8	4.93	0.011	15.61	0.04	81.6	21.71	0.06
4.5	218.169	0.210	11.476	0.021	0.187	0.001	30.808	0.039	0.1422	0.0010	0.253	9.3	5.26	0.012	15.60	0.05	81.9	21.69	0.07
5.0	270.781	0.160	14.588	0.011	0.238	0.001	47.794	0.055	0.1669	0.0009	0.321	11.8	6.42	0.009	15.48	0.03	83.2	21.53	0.04
5.5	182.259	0.160	9.713	0.019	0.162	0.001	37.299	0.058	0.1204	0.0010	0.214	7.9	7.53	0.019	15.45	0.05	82.2	21.50	0.07
6.0	200.268	0.180	10.712	0.017	0.176	0.002	48.824	0.126	0.1262	0.0010	0.236	8.7	8.93	0.027	15.63	0.05	83.4	21.75	0.06
10YV07, whole rock, J = 0.000776 ± 0.000003; UTM coordinates 336488, 4450171																				
0.5	223.120	0.750	28.556	0.070	0.439	0.002	5.029	0.008	0.3090	0.0016	0.629	19.1	0.35	0.001	4.63	0.04	59.3	6.47	0.05
0.8	119.640	0.240	20.447	0.041	0.287	0.002	5.645	0.010	0.1043	0.0009	0.450	13.7	0.54	0.001	4.37	0.02	74.6	6.10	0.03
1.2	95.087	0.160	18.449	0.018	0.250	0.002	8.067	0.020	0.0691	0.0006	0.406	12.3	0.86	0.002	4.08	0.01	79.2	5.71	0.02
1.5	76.535	0.085	14.515	0.018	0.203	0.001	6.479	0.012	0.0608	0.0006	0.320	9.7	0.87	0.002	4.07	0.02	77.2	5.69	0.02
1.8	53.934	0.064	9.815	0.013	0.140	0.001	4.104	0.010	0.0507	0.0006	0.216	6.6	0.82	0.002	4.00	0.02	72.8	5.59	0.03
2.1	35.885	0.054	6.507	0.009	0.094	0.001	3.471	0.010	0.0348	0.0005	0.143	4.4	1.05	0.003	3.98	0.03	72.1	5.56	0.04
2.5	28.483	0.038	5.526	0.009	0.080	0.001	5.535	0.014	0.0266	0.0005	0.122	3.7	1.96	0.006	3.82	0.03	74.0	5.33	0.04
3.0	89.339	0.073	14.529	0.016	0.228	0.001	21.915	0.034	0.1221	0.0007	0.320	9.7	2.96	0.006	3.79	0.02	61.6	5.30	0.02
3.5	130.794	0.120	18.666	0.019	0.311	0.002	35.905	0.085	0.2149	0.0010	0.411	12.5	3.77	0.010	3.77	0.02	53.7	5.26	0.03
4.0	38.868	0.049	5.379	0.009	0.089	0.001	13.248	0.027	0.0629	0.0006	0.118	3.6	4.83	0.013	3.98	0.04	54.9	5.56	0.05
4.5	15.360	0.018	2.099	0.005	0.037	0.001	6.847	0.034	0.0262	0.0005	0.046	1.4	6.39	0.036	3.90	0.07	53.2	5.45	0.10
5.0	9.825	0.017	1.352	0.004	0.022	0.001	7.650	0.014	0.0176	0.0005	0.030	0.9	11.09	0.042	3.89	0.11	53.3	5.43	0.16
5.5	13.800	0.020	1.856	0.006	0.029	0.001	11.277	0.042	0.0218	0.0005	0.041	1.2	11.91	0.061	4.48	0.09	60.0	6.25	0.12
6.0	18.757	0.029	1.828	0.005	0.033	0.001	13.461	0.027	0.0387	0.0006	0.040	1.2	14.43	0.052	4.63	0.11	44.9	6.46	0.15

Note: All data corrected for mass discrimination (= 1.008), blanks, radioactive decay, and interfering nucleogenic isotope reactions. Neutron flux (J) normalized to Fish Canyon sanidine with an age of 28.20 ± 0.09 Ma (Kuiper et al., 2008). Calculated ages with $^{40}Ar/^{36}Ar$ ratio of trapped argon equal to atmospheric value of 298.56 (Lee et al., 2006); isochron data indicate trapped values >300 (see text). Locations relative to North America Datum 27, zone 13.

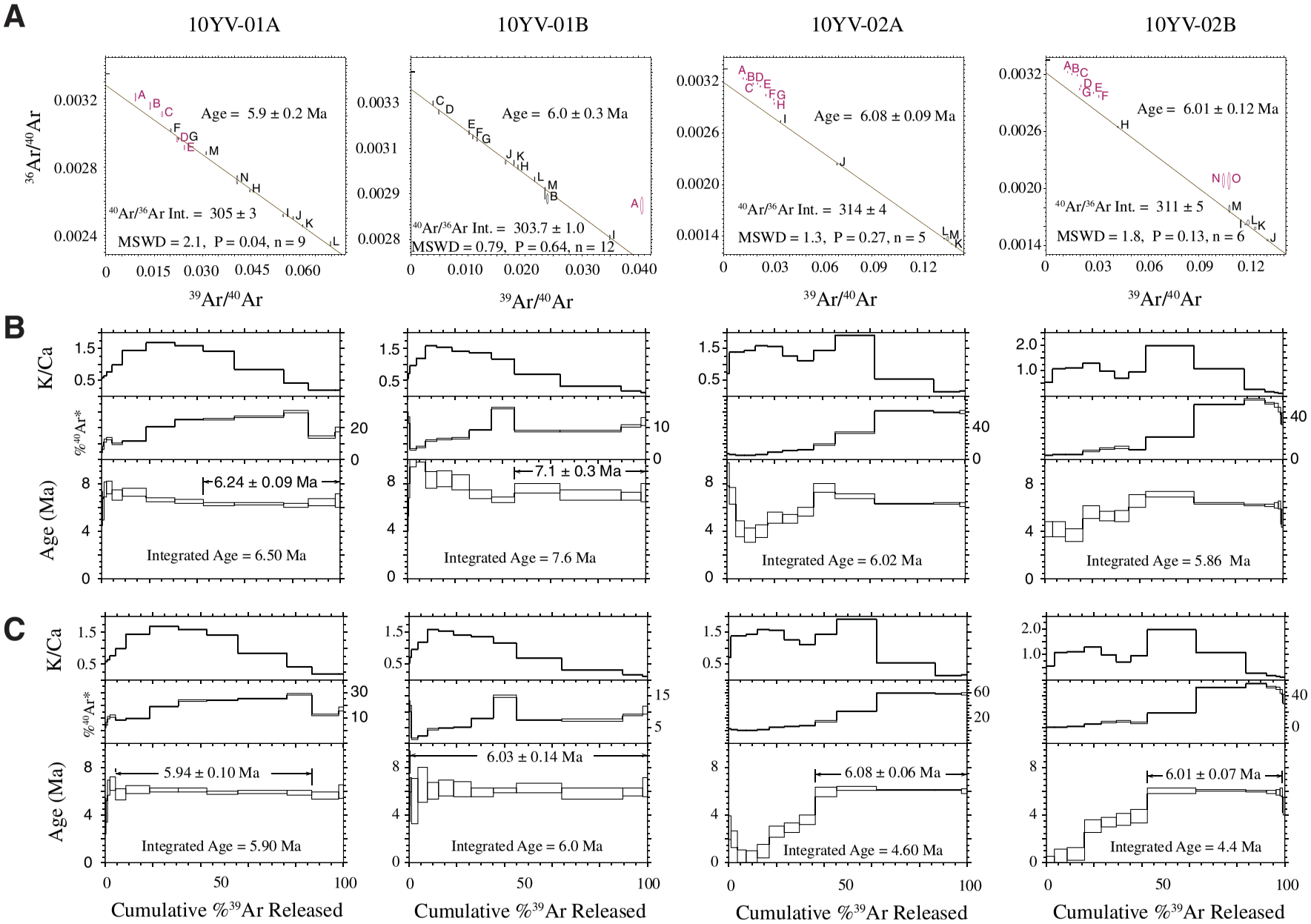

Figure 15 (*Continued on facing page*). Plots of $^{40}Ar/^{39}Ar$ CO_2-laser incremental-heating data from Yampa volcanic rock samples. (A) $^{39}Ar/^{40}Ar$ versus $^{36}Ar/^{40}Ar$ isochron plots. Note that the trapped $^{40}Ar/^{36}Ar$ values defined by the ordinate intercept are systematically >300, consistent with a nonatmospheric component of trapped argon. Isochron regresssions exclude analytical steps indicated in red. MSWD—mean square of weighted deviates; P—probability of fit. (B) Incremental-heating $^{40}Ar/^{39}Ar$ age spectra calculated using initial $^{40}Ar/^{36}Ar$ ratios equal to modern atmosphere (298.56). Radiogenic argon ($^{40}Ar^*$) and K/Ca ratios also plotted for reference.

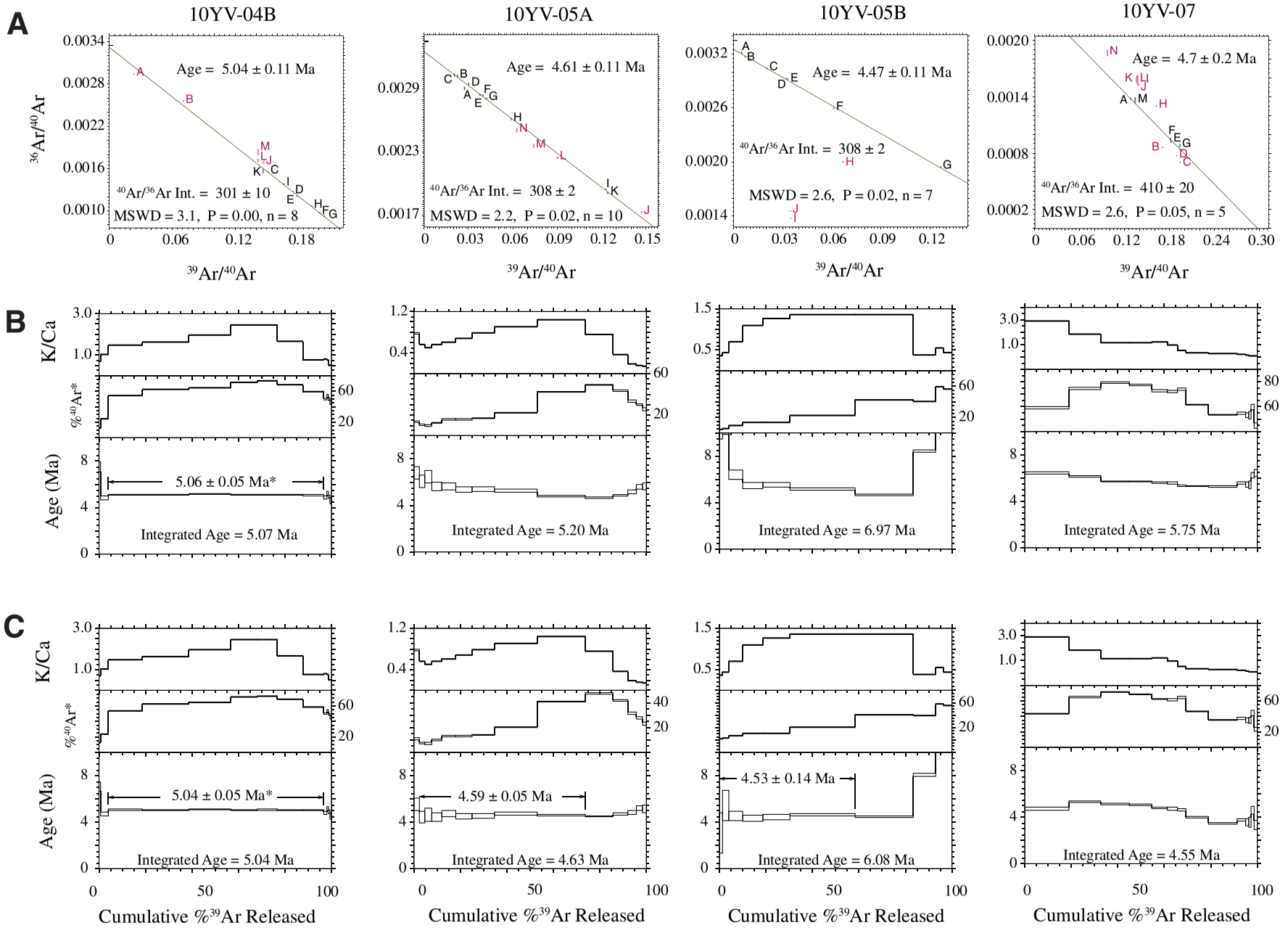

Figure 15 (*Continued*). Note the highly irregular shapes of the age spectra and lack of $^{40}Ar/^{39}Ar$ age plateaus. (C) Incremental-heating $^{40}Ar/^{39}Ar$ age spectra calculated using initial $^{40}Ar/^{36}Ar$ ratios defined by the ordinate intercept of the $^{39}Ar/^{40}Ar$ versus $^{36}Ar/^{40}Ar$ isochron plots. Sample 10YV-06 failed to yield a meaningful isochron plot and is excluded from this diagram; however, the data are reported in Table 4. All quoted errors, including the width of individual boxes on the $^{40}Ar/^{39}Ar$ age spectra, are 2σ.

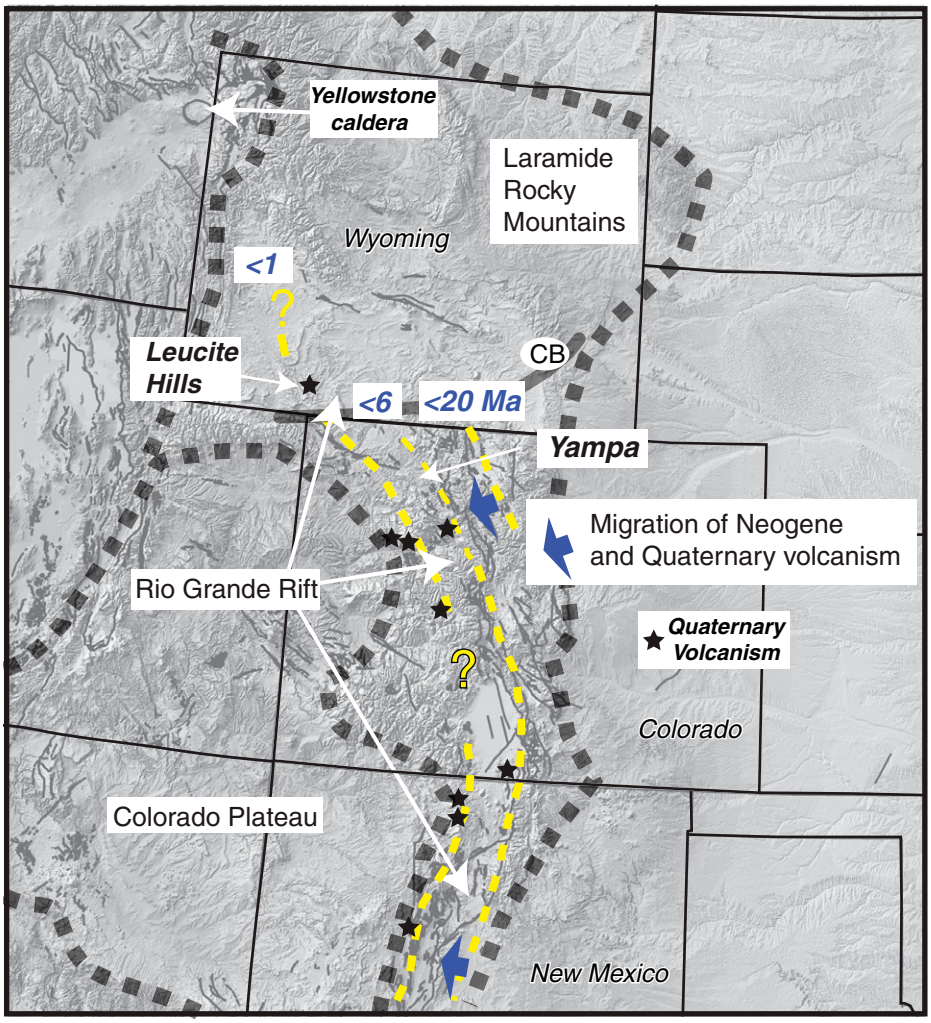

Figure 16. Regional age limits and migration of Neogene to Quaternary volcanism within the northern Rio Grande rift projected onto a digital elevation map with faults (black lines) indicating Neogene motion. Geochronologic data are from this study, data summarized in Izett (1975) and Leat et al. (1990), and our $^{40}Ar/^{39}Ar$ data from New Mexico and Colorado. Yellow dashed lines are eastern limits of active volcanism since 20 Ma. The present position of the northernmost Rio Grande rift is limited to the region west of the 6 Ma age limit and includes the Leucite Hills, Wyoming. Note the continuing westward migration of Pliocene and younger volcanism since late Miocene time toward the northeast margin of the Colorado Plateau. CB is the approximate position of the Cheyenne belt.

physiographic rift graben appeared ca. 10 Ma in the southern Rio Grande rift (McMillan et al., 2000) and ca. 6 Ma in the Rio Grande rift of southern Colorado (e.g., Lipman and Mehnert, 1975; Johnson and Thompson, 1991; Thompson et al., 2012). An asthenospheric source region for these basalts provides a simple distinction between rift-related magmatism and the earlier calc-alkaline magmatism and regional extension ~10 m.y. earlier. The Rio Grande rift is therefore interpreted as a late Miocene and younger physiographic feature (e.g., Prodehl and Lipman, 1989), distinct from the Oligocene and early Miocene regional extension and volcanic activity imprinted over much of western North America. Although published $^{176}Hf/^{177}Hf$ isotope ratios support subcontinental lithospheric mantle sources for most lavas of northwest Colorado (Beard and Johnson, 1993), it seems likely that the heat necessary to melt the subcontinental lithosphere is derived from infiltrating asthenospheric mantle. With the possible exception of the Yampa lavas, magmas sourced in the asthenospheric mantle have not yet definitively appeared in the northernmost segment of the Rio Grande rift in Colorado and Wyoming, but this system is still evolving, as evidenced by the Quaternary alkaline lavas distributed along a zone northeast of the Colorado Plateau, including the Leucite Hills (Fig. 16). The lack of a definitive asthenospheric mantle Hf isotopic signal may be due to the dynamic nature of the entire melting process, as these highly alkaline lavas represent the first melt fractions from a previously veined lithospheric mantle that developed during an earlier period of lithospheric deformation and partial melting.

SUMMARY AND IMPLICATIONS FOR THE NORTHERN RIO GRANDE RIFT

Lithospheric thickness is variable within the Rio Grande rift corridor but is notably thinner in the south than in the north (e.g., Prodehl and Lipman, 1989; Gao et al., 2004; Schmandt and Humphreys, 2010). Seismic tomography in the Rio Grande rift of southern New Mexico indicates a lithospheric mantle thickness of 45 km (e.g., Gao et al., 2004) and is thin enough to allow partial melts from the asthenospheric mantle to erupt at the surface (e.g., Harry and Leeman, 1995). Passive rifting alone does not account for thinning this initially thick (>100 km) lithosphere to 45 km, but more than 50% of the thinning could have occurred through mechanical abrasion and assimilation by the asthenospheric mantle (e.g., Gao et al., 2004; Byerly and Lassiter, 2012). In the northernmost Rio Grande rift (north of Leadville), the lithosphere is thicker than 100 km and present-day seismic tomography reveals anomalously slow P-wave traveltimes at a depth of 90 km, roughly coincident with an area approximately beneath the northern Rio Grande rift and extending from the northeastern margin of the Colorado Plateau into southern Wyoming (Yuan and Dueker, 2005; Schmandt and Humphreys, 2010). The seismic tomographic resolution is coarse, but seismic velocities in this region are indicative of melt at these depths, and may reflect asthenospheric mantle intrusion into, and current removal of, the subcontinental lithospheric mantle (e.g., Karlstrom et al., 2012). Although the available radiogenic isotope data support primarily lithospheric mantle sources for lavas of northwest Colorado (e.g., Beard and Johnson, 1993), there is some Nd and Hf isotopic evidence of an asthenospheric mantle source in the Yampa lavas, and continuing thinning of the subcontinental lithospheric mantle below northwest Colorado should lead to additional magmas originating in the asthenospheric mantle.

The Pliocene and younger alkalic volcanism along the northeast margin of the Colorado Plateau defines an overall northwest strike of the Rio Grande rift west of the Park Range that includes the Leucite Hills. This incipient northern Rio Grande rift projects broadly toward

the Snake River Plain hotspot track at Yellowstone, where asthenospheric mantle is present at much shallower depths (Christiansen, 2001). Although the Wyoming craton, a thick Archean lithospheric root (e.g., Humphreys and Dueker, 1994), is between Yellowstone and the northern Rio Grande rift, the southwestward migration of Pliocene and younger alkalic volcanism indicates that thinning of, and intrusion into, this lithospheric mantle by asthenospheric magmas should occur in the geologic future. Large-scale sutures, such as the southward-dipping Cheyenne belt separating Archean and Proterozoic lithosphere near the Wyoming-Colorado border (e.g., Karlstrom and Houston, 1984; Zurek and Dueker, 2005), are recognized seismically as imbrications that have remained intact since the Proterozoic (e.g., Hansen and Dueker, 2009). Given that asthenospheric magmas are observed along Proterozoic sutures of the southern margin of the Colorado Plateau (e.g., Karlstrom and Houston, 1984; Magnani et al., 2004; Crow et al., 2011), such melts will eventually intrude along the Cheyenne belt.

Magmas unequivocally derived by partial melting of asthenospheric mantle within the Rio Grande rift are younger than 10 Ma, cut across preexisting physical boundaries, and overprint evidence of earlier regional extension and associated calc-alkalic igneous activity (see also Ingersoll, 1982; Baldridge et al., 1991). The distribution of Quaternary basalts in the Rio Grande rift indicates that magmatism is continuing and migrating toward the eastern margin of the Colorado Plateau. In part because of its location along the eastern margin of the Colorado Plateau, the Rio Grande rift has been interpreted as an incipient spreading center that will ultimately lead to plate separation and subsequent creation of a Colorado Plateau microplate (Coney, 1987). The proximity and colinearity of the alkaline Yampa rocks and neighboring Pliocene to Quaternary lavas in northwestern Colorado and Wyoming with the block-faulted Rio Grande rift farther south supports a hypothesis that asthenospheric upwelling is following zones of lithospheric weakness developed during late Cenozoic extension and this system is continuing to evolve and propagate along the northeast Colorado Plateau margin in a northwestward direction toward Yellowstone.

ACKNOWLEDGMENTS

We gratefully acknowledge U.S. Geological Survey (USGS) colleagues Celeste Mercer, Heather Lowers, and Renee Pillers for assistance with the electron microbeam measurements and Jim Budahn for the X-ray fluorescence analyses. We thank the USGS TRIGA reactor staff for their assistance with sample irradiations, and Jennifer Sliney for introducing Cosca to the region near Yampa, Colorado. Discussions with and comments by USGS colleagues Jonathan Caine, Jim Cole, Ed du Bray, and Ed DeWitt helped formulate some of the ideas presented here, and Janet Slate provided valuable proofreading. We also thank two anonymous journal reviewers for constructive comments. Any use of trade, product, or firm names is for descriptive purposes only and does not imply endorsement by the U.S. Government.

REFERENCES CITED

Atwater, T., and Stock, J.M., 1998, Pacific–North America plate tectonics of the Neogene southwestern United States: An update: International Geology Review, v. 40, p. 375–402, doi:10.1080/00206819809465216.

Baldridge, W.S., Perry, F.V., Vaniman, D.T., Nealy, L.D., Leavy, B.D., Laughlin, A.W., Kyle, P., Bartov, Y., Steinitz, G., and Gladney, G.S., 1991, Middle to late Cenozoic magmatism of the southeastern Colorado Plateau and central Rio Grande rift (New Mexico and Arizona, USA): A model for continental rifting: Tectonophysics, v. 197, p. 327–354, doi:10.1016/0040-1951(91)90049-X.

Beard, B.L., and Johnson, C.M., 1993, Hf isotope composition of late Cenozoic basaltic rocks from northwestern Colorado, USA: New constraints on mantle enrichment processes: Earth and Planetary Science Letters, v. 119, p. 495–509, doi:10.1016/0012-821X(93)90058-H.

Berglund, H.T., Sheehan, A.F., Murray, M.H., Roy, M., Lowry, A.R., Nerem, R.S., and Blume, F., 2012, Distributed deformation across the Rio Grande rift, Great Plains, and Colorado Plateau: Geology, v. 40, p. 23–26, doi:10.1130/G32418.1.

Byerly, B.L., and Lassiter, J.C., 2012, Evidence from mantle xenoliths for lithosphere removal beneath the central Rio Grande rift: Earth and Planetary Science Letters, v. 355–356, p. 82–93, doi:10.1016/j.epsl.2012.08.034.

Carmichael, I.S.E., 1967, The mineralogy and petrology of volcanic rocks from the Leucite Hills, Wyoming: Contributions to Mineralogy and Petrology, v. 15, p. 24–66, doi:10.1007/BF01167214.

Carmichael, I.S.E., Luhr, J.F., and Lange, R.A., 1996, Quaternary minettes and associated volcanic rocks of Mascota, western Mexico: A consequence of plate extension above a subduction modified mantle wedge: Contributions to Mineralogy and Petrology, v. 124, p. 302–333, doi:10.1007/s004100050193.

Chamberlain, C.P., Mix, H.T., Mulch, A., Hren, M.T., Kent-Corson, M.L., Davis, S.J., Horton, T.W., and Graham, S.A., 2012, The Cenozoic climatic and topographic evolution of the western North American Cordillera: American Journal of Science, v. 312, p. 213–262, doi:10.2475/02.2012.05.

Chapin, C.E., 1979, Evolution of the Rio Grande rift—A summary, *in* Riecker, R.E., ed., Rio Grande Rift: Tectonics and magmatism: American Geophysical Union Special Publication 14, p. 1–6, doi:10.1029/SP014p0001.

Chapin, C.E., 2012, Origin of the Colorado Mineral Belt: Geosphere, v. 8, p. 28–43, doi:10.1130/GES00694.1.

Christiansen, R.L., 2001, The Quaternary and Pliocene Yellowstone Plateau volcanic field of Wyoming, Idaho, and Montana: U.S. Geological Survey Professional Paper 729-G, 120 p.

Christiansen, R.L., and Yeats, R.S., 1992, Post-Laramide geology of the U.S. Cordilleran region, *in* Burchfiel, B.C., et al., eds., The Cordilleran orogen: Conterminous U.S.: Boulder, Colorado, Geological Society of America, Geology of North America, v. G-3, p. 261–406.

Cole, J.C., Trexler, J.H., Cashman, P.H., Miller, I., Shroba, R.R., Cosca, M.A., and Workman, J.B., 2010, Beyond Colorado's Front Range: A new look at Laramide basin subsidence, sedimentation, and deformation in north-central Colorado, *in* Morgan, L.A., and Quane, S.L., eds., Through the generations: Geologic and anthropogenic field excursions in the Rocky Mountains from modern to ancient: Geological Society of America Field Guide 18, p. 55–76, doi:10.1130/2010.0018(03).

Coney, P.J., 1987, The regional tectonic setting and possible causes of Cenozoic extension in the North American Cordillera, *in* Coward, M.P., e al., eds., Continental extensional tectonics: Geological Society of London Special Publication 28, p. 177–186, doi:10.1144/GSL.SP.1987.028.01.13.

Crow, R., Karlstrom, K., Asmerom, Y., Schmandt, B., Polyak, V., and DuFrane, S.A., 2011, Shrinking of the Colorado Plateau via lithospheric mantle erosion: Evidence from Nd and Sr isotopes and geochronology of Neogene basalts: Geology, v. 39, p. 27–30, doi:10.1130/G31611.1.

Dickinson, W.R., 2002, The Basin and Range province as a composite extensional domain: International Geology Review, v. 44, p. 1–38, doi:10.2747/0020-6814.44.1.1.

Dickinson, W.R., 2004, Evolution of the North American Cordillera: Annual Review of Earth and Planetary Sciences, v. 32, p. 13–45, doi:10.1146/annurev.earth.32.101802.120257.

Dueker, K., Yuan, H., and Zurek, B., 2001, Thick-structured Proterozoic lithosphere of the Rocky Mountain region: GSA Today, v. 11, p. 4–9, doi:10.1130/1052-5173(2001)011<0004:TSPLOT>2.0.CO;2.

Eaton, G.P., 2008, Epeirogeny in the southern Rocky Mountains region: Evidence and origin: Geosphere, v. 4, p. 764–784, doi:10.1130/GES00149.1.

Edgar, A.D., 1987, The genesis of alkaline magmas with emphasis on their source regions: Inferences from experimental studies, *in* Fitton, J.G., and Upton, B.G.J., eds., Alkaline igneous rocks: Geological Society of London Special Publication 30, p. 29–52, doi:10.1144/GSL.SP.1987.030.01.04.

Foley, S., 1992, Vein-plus-wall-rock melting mechanisms in the lithosphere and the origin of potassic alkaline magmas: Lithos, v. 28, p. 435–453, doi:10.1016/0024-4937(92)90018-T.

Foley, S.F., Barth, M.G., and Jenner, G.A., 2000, Rutile/melt partition coefficients for trace elements and an assessment of the influence of rutile on the trace element characteristics of subduction zone magmas: Geochimica et Cosmochimica Acta, v. 64, p. 933–938, doi:10.1016/S0016-7037(99)00355-5.

Gao, W., Grand, S.P., Baldridge, W.S., Wilson, D., West, M., Ni, J.F., and Aster, R., 2004, Upper mantle convection beneath the central Rio Grande rift imaged by P and S wave tomography: Journal of Geophysical Research, v. 109, B03305, doi:10.1029/2003JB002743.

Giegengack, R.F., 1962, Recent volcanism near Dotsero, Colorado [M.S. thesis]: Boulder, University of Colorado, 69 p.

Gonzales, D.A., Turner, B.E., Burgess, R.T., Holnback, C.C., and Critchley, M.R., 2010, New insight into the timing and history of diatreme-dike complexes of the northeastern Navajo volcanic field, southwestern Colorado, *in* Four Corners country: New Mexico Geological Society 61st Field Conference Guidebook, p. 163–172.

Hansen, S., and Dueker, K., 2009, P- and S-wave receiver function images of crustal imbrication beneath the Cheyenne Belt in southeast Wyoming: Seismological Society of America Bulletin, v. 99, p. 1953–1961, doi:10.1785/0120080168.

Harry, D.L., and Leeman, W.P., 1995, Partial melting of melt-metasomatized subcontinental mantle and the magma source potential of the lower lithosphere: Journal of Geophysical Research, v. 100, p. 10255–10269, doi:10.1029/94JB03065.

Hills, F.A., and Houston, R.S., 1979, Early Proterozoic tectonics of the central Rocky Mountains, North America: Contributions to Geology (Copenhagen), v. 17, p. 89.

Humphreys, E.D., 1995, Post-Laramide removal of the Farallon slab, western United States: Geology, v. 23, p. 987–990, doi:10.1130/0091-7613(1995)023<0987:PLROTF>2.3.CO;2.

Humphreys, E., 2009, Relation of flat slab subduction to magmatism and deformation in the western United States, *in* Kay, S.M., et al., eds., Backbone of the Americas: Shallow subduction, plateau uplift, and ridge and terrane collision: Geological Society of America Memoir 204, p. 85–98, doi:10.1130/2009.1204(04).

Humphreys, E.D., and Dueker, K.G., 1994, Western U.S. upper mantle structure: Journal of Geophysical Research, v. 99, p. 9615–9634, doi:10.1029/93JB01724.

Humphreys, E., Hessler, E., Dueker, K., Erslev, E., Farmer, G.L., and Atwater, T., 2003, How Laramide-age hydration of North America by the Farallon slab controlled subsequent activity in the western U.S: International

Geology Review, v. 45, p. 575–595, doi:10.2747/0020-6814.45.7.575.

Ingersoll, R.V., 1982, Triple-junction instability as cause for late Cenozoic extension and fragmentation of the western United States: Geology, v. 10, p. 621–624, doi:10.1130/0091-7613(1982)10<621:TIACFL>2.0.CO;2.

Ingersoll, R.V., 2001, Structural and stratigraphic evolution of the Rio Grande rift, northern New Mexico and southern Colorado: International Geology Review, v. 43, p. 867–891, doi:10.1080/00206810109465053.

Izett, G.A., 1975, Late Cenozoic sedimentation and deformation in northern Colorado and adjoining areas, *in* Curtis, B.F., ed., Cenozoic history of the southern Rocky Mountains: Geological Society of America Memoir 144, p. 179–210, doi:10.1130/MEM144-p179.

Johnson, C.M., and Beard, B.L., 1993, Evidence from hafnium isotopes for ancient sub-oceanic mantle beneath the Rio Grande rift: Nature, v. 362, p. 441–444, doi:10.1038/362441a0.

Johnson, C.M., and Thompson, R.A., 1991, Isotopic composition of Oligocene mafic volcanic rocks in the northern Rio Grande rift: Evidence for contributions of ancient intraplate and subduction magmatism to evolution of the lithosphere: Journal of Geophysical Research, v. 96, p. 13593–13608, doi:10.1029/91JB00342.

Jones, C.H., Wernicke, B.P., Farmer, G.L., Walker, J.D., Coleman, D.S., McKenna, L.W., and Perry, F.V., 1992, Variations across and along a major continental rift: An interdisciplinary study of the Basin and Range province, western USA: Tectonophysics, v. 213, p. 57–96, doi:10.1016/0040-1951(92)90252-2.

Jones, C.H., Farmer, G.L., Sageman, B., and Zhong, S., 2011a, Hydrodynamic mechanism for the Laramide orogeny: Geosphere, v. 7, p. 183–201, doi:10.1130/GES00575.1.

Jones, D.S., Barnes, C.G., Premo, W.R., and Snoke, A.W., 2011b, The geochemistry and petrogenesis of the Paleoproterozoic Green Mountain arc: A composite(?), bimodal, oceanic, fringing arc: Precambrian Research, v. 185, p. 231–249, doi:10.1016/j.precamres.2011.01.011.

Karlstrom, K.E., and Houston, R.S., 1984, The Cheyenne Belt: Analysis of a Proterozoic suture in southern Wyoming: Precambrian Research, v. 25, p. 415–446, doi:10.1016/0301-9268(84)90012-3.

Karlstrom, K.E., 23 others, and the CREST Working Group, 2012, Mantle-driven dynamic uplift of the Rocky Mountains and Colorado Plateau and its surface response: Toward a unified hypothesis: Lithosphere, v. 4, p. 3–22, doi:10.1130/L150.1.

Konzett, J., and Ulmer, P., 1999, The stability of hydrous potassic phases in lherzolitic mantle—An experimental study to 9.5 GPa in simplified and natural bulk compositions: Journal of Petrology, v. 40, p. 629–652, doi:10.1093/petroj/40.4.629.

Kuiper, K.F., Deino, A., Hilgen, F.J., Krijgsman, W., Renne, P.R., and Wijbrans, J.R., 2008, Synchronizing rock clocks of Earth history: Science, v. 320, p. 500–504, doi:10.1126/science.1154339.

Lange, R.A., Carmichael, I.S.E., and Hall, C.M., 2000, $^{40}Ar/^{39}Ar$ chronology of the Leucite Hills, Wyoming: Eruption rates, erosion rates, and an evolving temperature structure of the underlying mantle: Earth and Planetary Science Letters, v. 174, p. 329–340, doi:10.1016/S0012-821X(99)00267-8.

Larson, E.E., Ozima, M., and Bradley, W.C., 1975, Late Cenozoic basic volcanism in northwestern Colorado and its implications concerning tectonism and the origin of the Colorado River system, *in* Curtis, B.F., ed., Cenozoic history of the southern Rocky Mountains: Geological Society of America Memoir 144, p. 155–178, doi:10.1130/MEM144-p155.

Leat, P.T., and Thompson, R.N., 1988, Miocene hydrovolcanism in NW Colorado, USA, fueled by explosive mixing of basic magma and wet unconsolidated sediment: Bulletin of Volcanology, v. 50, p. 229–243, doi:10.1007/BF01047486.

Leat, P.T., Thompson, R.N., Morrison, M.A., Hendry, G.L., and Dickin, A.P., 1988, Compositionally-diverse Miocene-Recent rift-related magmatism in northwest Colorado: Partial melting, and mixing of mafic magmas from 3 different asthenospheric and lithospheric mantle sources: Journal of Petrology, Special Lithosphere Issue, p. 351–377, doi:10.1093/petrology/Special_Volume.1.351.

Leat, P.T., Thompson, R.N., Dickin, A.P., Morrison, M.A., and Hendry, G.L., 1989, Quaternary volcanism in northwestern Colorado: Implications for the roles of asthenosphere and lithosphere in the genesis of continental basalts: Journal of Volcanology and Geothermal Research, v. 37, p. 291–310, doi:10.1016/0377-0273(89)90085-1.

Leat, P.T., Thompson, R.N., Morrison, M.A., Hendry, G.L., and Dickin, A.P., 1990, Geochemistry of mafic lavas in the early Rio Grande rift, Yarmony Mountain, Colorado, U.S.A: Chemical Geology, v. 81, p. 23–43, doi:10.1016/0009-2541(90)90037-8.

Leat, P.T., Thompson, R.N., Morrison, M.A., Hendry, G.L., and Dickin, A.P., 1991, Alkaline hybrid mafic magmas of the Yampa area, NW Colorado, and their relationship to the Yellowstone mantle plume and lithospheric mantle domains: Contributions to Mineralogy and Petrology, v. 107, p. 310–327, doi:10.1007/BF00325101.

Lee, J.-Y., Marti, K., Severinghaus, J.P., Kawamura, K., Yoo, H.-S., Lee, J.B., and Kim, J.S., 2006, A redetermination of the isotopic abundances of atmospheric Ar: Geochimica et Cosmochimica Acta, v. 70, p. 4507–4512, doi:10.1016/j.gca.2006.06.1563.

Le Maitre, R.W., Bateman, P., Dudek, A., Keller, J., Lameyre, J., Le Bas, M.J., Sabine, P.A., Schmid, R., Sorensen, H., Streckeisen, A., Woolley, A.R., and Zanettin, B., 1989, A classification of igneous rocks and glossary of terms: Recommendations of the International Union of Geological Sciences Subcommission on the Systematics of Igneous Rocks: Oxford, U.K., Blackwell Scientific Publications, 193 p.

Lipman, P.W., 1969, Alkalic and thoeliitic basaltic volcanism related to the Rio Grande depression, southern Colorado and northern New Mexico: Geological Society of America Bulletin, v. 80, p. 1343–1354, doi:10.1130/0016-7606(1969)80[1343:AATBVR]2.0.CO;2.

Lipman, P.W., and McIntosh, W.C., 2008, Eruptive and noneruptive calderas, northeastern San Juan Mountains, Colorado: Where did the ignimbrites come from?: Geological Society of America Bulletin, v. 120, p. 771–795, doi:10.1130/B26330.1.

Lipman, P.W., and Mehnert, H., 1975, Late Cenozoic basaltic volcanism and development of the Rio Grande depression in the southern Rocky Mountains, *in* Curtis, B.F., ed., Cenozoic history of the southern Rocky Mountains: Geological Society of America Memoir 144, p. 119–154, doi:10.1130/MEM144-p119.

Lipman, P.W., Prostka, H.J., and Christiansen, R.L., 1971, Evolving subduction zones in the western United States, as interpreted from igneous rocks: Science, v. 174, p. 821–825, doi:10.1126/science.174.4011.821.

Lloyd, F.E., and Bailey, D.K., 1975, Light element metasomatism of the continental mantle: The evidence and the consequences: Physics and Chemistry of the Earth, v. 9, p. 389–416, doi:10.1016/0079-1946(75)90030-0.

Ludwig, K.R., 1992, User's manual for ANALYST version 2.20: An IBM-PC computer program for control of a thermal-ionization, single-collector mass-spectrometer: U.S. Geological Survey Open-File Report 92–543, 89 p.

Ludwig, K.R., 2003, User's manual for Isoplot/Ex 3.00: A geochronological toolkit for Microsoft Excel: Berkeley Geochronological Center Special Publication 4, 70 p.

Lugmair, G.W., Scheinin, N.B., and Marti, K., 1975, Sm-Nd age and history of Apollo 17 basalt 75075: Evidence for early differentiation of the lunar exterior: Proceedings of the 6th Lunar Science Conference, Volume 2: New York, Pergamon Press, Inc., p. 1419–1429.

Magnani, M.B., Miller, K.C., Levander, A., and Karlstrom, K., 2004, The Yavapai-Mazatzal boundary: A long-lived tectonic element in the lithosphere of southwestern North America: Geological Society of America Bulletin, v. 116, p. 1137–1142, doi:10.1130/B25414.1.

McIntosh, W.C., and Chapin, C.E., 2004, Geochronology of the central Colorado volcanic field: New Mexico Bureau of Geology and Mineral Resources Bulletin, v. 160, p. 205–237.

McMillan, N.J., Dickin, A.P., and Haag, D., 2000, Evolution of magma source regions in the Rio Grande rift, southern New Mexico: Geological Society of America Bulletin, v. 112, p. 1582–1593, doi:10.1130/0016-7606(2000)112<1582:EOMSRI>2.0.CO;2.

Mirnejad, H., and Bell, K., 2006, Origin and source evolution of the Leucite Hills lamproites: Evidence from Sr-Nd-Pb-O isotopic compositions: Journal of Petrology, v. 47, p. 2463–2489, doi:10.1093/petrology/egl051.

Pilet, S., Baker, M.B., Müntener, O., and Stolper, E.M., 2011, Monte Carlo simulations of metasomatic enrichment in the lithosphere and implications for the source of alkaline basalts: Journal of Petrology, v. 52, p. 1415–1442, doi:10.1093/petrology/egr007.

Premo, W.R., and Loucks, R.R., 2000, Age and Pb-Sr-Nd isotopic systematics of plutonic rocks from the Green Mountain magmatic arc, southeastern Wyoming: Isotopic characterization of a Paleoproterozoic island arc system: Rocky Mountain Geology, v. 35, p. 51–70, doi:10.2113/35.1.51.

Premo, W.R., and Van Schmus, W.R., 1989, Zircon geochronology of Precambrian rocks in southeastern Wyoming and northern Colorado, *in* Grambling, J.A., and Tewksbury, B.J., eds., Proterozoic geology of the southern Rocky Mountains: Geological Society of America Special Paper 235, p. 13–32, doi:10.1130/SPE235-p13.

Prodehl, C., and Lipman, P.W., 1989, Crustal structure of the Rocky Mountain region, *in* Pakiser, L.C., and Mooney, W.D., eds., Geophysical framework of the continental United States: Geological Society of America Memoir 172, p. 249–284, doi:10.1130/MEM172-p249.

Roy, M., Jordan, T.H., and Pederson, J., 2009, Colorado Plateau magmatism and uplift by warming of heterogeneous lithosphere: Nature, v. 459, p. 978–982, doi:10.1038/nature08052.

Schmandt, B., and Humphreys, E., 2010, Complex subduction and small-scale convection revealed by body-wave tomography of the western United States upper mantle: Earth and Planetary Science Letters, v. 297, p. 435–445, doi:10.1016/j.epsl.2010.06.047.

Schmidt, K., Bottazzi, P., Vannucci, R., and Mengel, K., 1999, Trace element partitioning between phlogopite, clinopyroxene and leucite lamproite melt: Earth and Planetary Science Letters, v. 168, p. 287–299, doi:10.1016/S0012-821X(99)00056-4.

Sonder, L.J., and Jones, C.H., 1999, Western United States extension: How the west was widened: Annual Review of Earth and Planetary Sciences, v. 27, p. 417–462, doi:10.1146/annurev.earth.27.1.417.

Stacey, J.S., and Kramers, J.D., 1975, Approximation of terrestrial lead isotope evolution by a 2-stage model: Earth and Planetary Science Letters, v. 26, p. 207–221, doi:10.1016/0012-821X(75)90088-6.

Sun, S.S., and McDonough, W.F., 1989, Chemical and isotopic systematics of oceanic basalts: Implications for mantle composition and processes, *in* Saunders, A.D., and Norry, M.J., eds., Magmatism in the ocean basins: Geological Society of London Special Publication 43, p. 313–345, doi:10.1144/GSL.SP.1989.042.01.19.

Tatsumoto, M., and Unruh, D.M., 1976, KREEP basalt age: Grain by grain U-Th-Pb systematics study of the quartz monzodiorite clast 15405: Proceedings of the 7th Lunar Science Conference, Volume 2: New York, Pergamon Press, Inc., p. 2107–2129.

Thompson, R.A., Turner, K.J., Cosca, M.A., Drenth, B.J., and Ruleman, C.A., 2012, Integrated geologic, geochronologic and geophysical studies of the northeastern Taos Plateau, New Mexico, USA; new constraints on the evolution of rift structures, basin evolution, and Pliocene volcanic eruption history: Geological Society of America Abstracts with Programs, v. 44, no. 6, p. 15.

Thompson, R.L., Leat, P.T., Dickin, A.P., Morrison, M.A., Hendry, G.L., and Gibson, S.A., 1990, Strongly potassic mafic magmas from lithospheric mantle sources during continental extension and heating: Evidence from Miocene minettes of north-west Colorado, U.S.A: Earth and Planetary Science Letters, v. 98, p. 139–153, doi:10.1016/0012-821X(90)90055-3.

Thompson, R.L., Gibson, S.A., Leat, P.T., Mitchell, J.G., Morrison, M.A., Hendry, G.L., and Dickin, A.P., 1993, Early Miocene extension-related basaltic magmatism at Walton Peak, northwest Colorado: Further evidence on continental basaltic magmatism: Geological Society of London Journal, v. 150, p. 277–292, doi:10.1144/gsjgs.150.2.0277.

Thompson, R.L., Velde, B., Morrison, M.A., Mitchell, J.G., Dickin, A.P., and Gibson, S.A., 1997, Oligocene lamproite containing an Al-poor, Ti-rich biotite, Middle Park, northwest Colorado, USA: Mineralogical Magazine, v. 61, p. 557–572, doi:10.1180/minmag.1997.061.407.08.

Tweto, O., 1979, The Rio Grande rift system in Colorado, *in* Riecker, R.E., ed., Rio Grande Rift: Tectonics and magmatism: American Geophysical Union Special Publication 14, p. 33–56, doi:10.1029/SP014p0033.

Wenrich, K.J., Billingsley, G.H., and Blackerby, B.A., 1995, Spatial migration and compositional changes of Miocene–Quaternary magmatism in the western Grand Canyon: Magnetism and extension: Journal of Geophysical Research, v. 100, no. B6, p. 10417–10440, doi:10.1029/95JB00373.

Wernicke, B.P., Christiansen, R.L., England, P.C., and Sonder, L.J., 1987, Tectonomagmatic evolution of Cenozoic extension in the North American Cordillera, *in* Coward, M.P., et al., eds., Continental extensional tectonics: Geological Society of London Special Publication 28, p. 203–221, doi:10.1144/GSL.SP.1987.028.01.15.

Williams, P.L., and Cole, J.C., 2007, Geologic map of the Albuquerque 30' × 60' quadrangle, north-central New Mexico: U.S. Geological Survey Scientific Investigations Map 2946, 31 p., scale 1:100,000.

York, D., Strangway, D.W., and Larson, E.E., 1971, Preliminary study of a Tertiary magnetic transition in Colorado: Earth and Planetary Science Letters, v. 11, p. 333–338, doi:10.1016/0012-821X(71)90188-9.

Yuan, H., and Dueker, K., 2005, Upper mantle tomographic Vp and Vs images of the Rocky Mountains in Wyoming, Colorado, and New Mexico: Evidence for a thick heterogeneous chemical lithosphere, *in* Karlstrom, K.E., and Keller, G.R., eds., The Rocky Mountain region—An evolving lithosphere: Tectonics, geochemistry and geophysics: American Geophysical Union Geophysical Monograph 154, p. 329–346, doi:10.1029/154GM25.

Zurek, B., and Dueker, K., 2005, Lithospheric stratigraphy beneath the southern Rocky Mountains, USA, *in* Karlstrom, K.E., and Keller, G.R., eds., The Rocky Mountain region—An evolving lithosphere: Tectonics, geochemistry and geophysics: American Geophysical Union Geophysical Monograph 154, p. 317–328, doi:10.1029/154GM24.